
This manuscript is a preprint and has been formally accepted for publication in the
Journal of Marine and Petroleum Geology.

The Influence of Base-Salt Relief, Rift Topography and Regional Events on Salt Tectonics Offshore Morocco

*Leonardo M. Pichel^{1,2}; Mads Huuse¹, Jonathan Redfern^{1,2}, Emma Finch¹

1 – School of Earth and Environmental Sciences, University of Manchester, Oxford Road, Manchester M13 9PL, UK

2 – North Africa Research Group, University of Manchester, Oxford Road, Manchester M13 9PL, UK

Key-words: SALT TECTONICS, DIAPIRISM, ALOCHTHONOUS SALT, SALT SHEETS, MINIBASIN, BASE-SALT RELIEF, RAMP-SYNCLINE BASINS, MOROCCO

ABSTRACT

1 This study integrates borehole-calibrated 2D and 3D seismic interpretation with
2 numerical models to provide a regional analysis of the complex salt tectonics offshore
3 central Morocco. We investigate the mechanisms controlling along-margin structural
4 variations, the effects of thick-skinned shortening and the sequential evolution of
5 allochthonous sheets. Additionally, we analyse how base-salt relief generated complex
6 flow kinematics and alternation of extensional and contractional domains by causing
7 flux variations at both autochthonous and allochthonous salt levels. The area is divided
8 into three structural provinces, with the central, Essaouira segment, having greater
9 downdip translation, structural complexity and volume of allochthonous salt, which
10 suggests the salt was originally thicker and better connected across multiple syn-rift
11 structures. The southern segment, Agadir, is dominated by up-right squeezed diapirs
12 formed by early load-driven rise and late shortening; limited salt and overburden
13 translation and no allochthonous sheets. The northern segment, Safi, is narrower and
14 has a smaller number of salt structures that were affected by abrupt translation due to
15 steep detachment gradient. Late, oblique thick-skinned shortening generated
16 contractional structures in the entire salt basin, which are most prominently developed
17 in Essaouira due to a favourably-oriented NW-SE syn-rift structure, the Talfeney
18 Accommodation Zone. Allochthonous salt sheets formed during four phases from the
19 Albian, Late Cretaceous, Paleocene to Oligo-Miocene by two main mechanisms:
20 contraction and basinward salt expulsion. This work improves understanding of the
21 structural configuration along the Moroccan margin guiding the identification of
22 potential sub-salt plays and contributing to a better comprehension of salt-related
23 deformation along rifted passive margins worldwide.

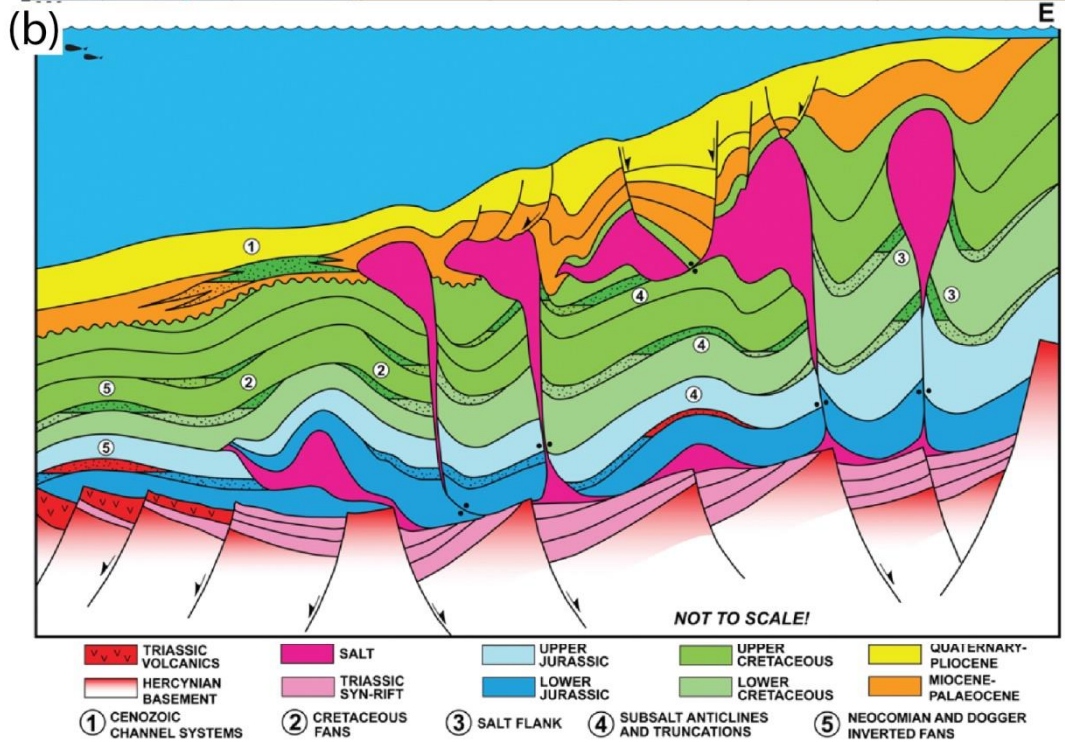
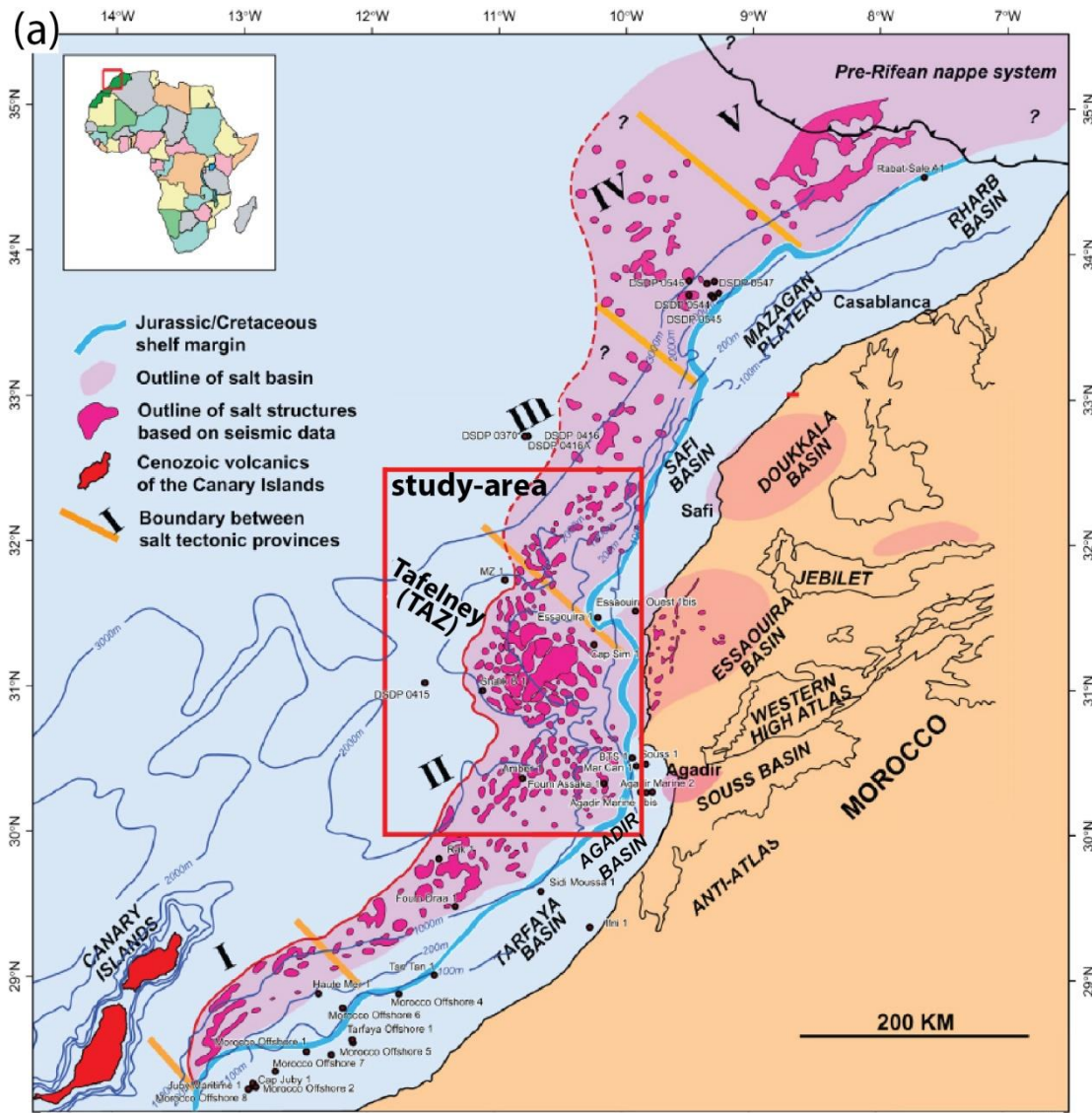
1. Introduction

24 The Moroccan Atlantic margin contains the longest (c. 1000 km) and widest (50-150
25 km) salt basin of NW Africa (Tari et al., 2003; 2017; Davison, 2005). The basin is
26 characterized by prominent along-strike variations in salt-related structural styles and
27 basin geometry (Fig. 1a), being divided into five distinct structural domains (Tari et al.,
28 2003; 2012). Salt was deposited from the Late Triassic to early Jurassic during the Early
29 Jurassic break-up of the African and North American plates (Tari et al, 2003; Davison et
30 al., 2005). Similar to the conjugate margin offshore Nova Scotia (Albertz et al., 2010;
31 Deptuck and Kendall 2017) and other Atlantic margin basins (e.g. Parentis Basin, Ferrer
32 et al., 2012), the salt in Morocco is interpreted to be late syn-rift (Tari et al., 2003; 2012;
33 Tari and Jabour, 2013; Davison et al., 2005). The syn-rift deposition resulted in thicker
34 salt in the hangingwall of predominantly NNE-NE half-grabens and thinner to non-
35 existent salt over their footwalls; ultimately producing a discontinuous salt interval
36 across the basin (Tari et al., 2003; Tari and Jabour 2013). Owing to complex salt
37 deformation, its syn-rift nature and the lack of deep-well penetrations of the
38 autochthonous salt, estimates of the original salt thickness are uncertain, ranging
39 between a few hundred meters (Tari et al., 2017) to over 1.5 km (Davison et al., 2005)
40 in their thickest portions.

41 Petroleum systems have been documented onshore Morocco, in the Essaouira-Agadir
42 Basin (Jabour et al., 2004; Tari and Jabour, 2013) but the offshore part of the margin
43 remains relatively sparsely explored, with no commercial discoveries to date. On the
44 conjugate margin in Nova Scotia, however, a number of fields have been discovered
45 along the shelf and deep-waters exploration is ongoing (Tari et al., 2012). Many salt-
46 related plays have been proposed (Tari et al., 2012; Tari and Jabour, 2013) but most of

47 them remain untested, suggesting there may be still untouched exploration potential
48 along the margin (Fig. 1b). Despite the lack of proven reservoir-quality sediments in the
49 Upper Cretaceous and Cenozoic targets, many regional elements point to the presence
50 of turbiditic deepwater fans in the Lower Cretaceous and Middle Jurassic (Lancelot and
51 Winterer, 1980; Tari et al., 2012). More recent studies also document the existence of
52 fluvial feeder systems that could be the source for deepwater fans in the Lower
53 Cretaceous (Luber et al., 2017; 2019). Due to the long-lived and dynamic salt
54 deformation (Hafid et al., 2000; Tari et al., 2003; 2012; Davison 2005), salt has acted as
55 a strong control in the distribution of depocentres and sediment fairways across the
56 slope and deep-basin, generating potential hydrocarbon traps and migration pathways.
57 Thus, understanding the controls, timing, kinematics and distribution of salt-related
58 structures is critical to de-risk deep-water hydrocarbon exploration in the area.

59 As a consequence of the limited availability of high-resolution seismic data and deep-
60 water wells, salt tectonics offshore Morocco and in most syn-rift salt basins (Tari et al.,
61 2003; Davison et al., 2005), is relatively less well understood compared with their post-
62 rift counterparts in the Gulf of Mexico and South Atlantic (Hudec and Jackson., 2004;
63 Rowan et al., 2004; Davison et al., 2012; Quirk et al., 2012; Hudec et al., 2013; Peel,
64 2014b; Rowan 2014; 2018; Jackson et al., 2015a,b). The variety of salt-related structural
65 styles and interaction with complex basin geometries make Morocco one of the most
66 interesting places to study salt tectonics, especially in light of recent modelling advances
67 and novel aspects of effects of pre-salt relief on salt flow (Dooley and Hudec, 2016;
68 Dooley et al., 2016; 2018; Ferrer et al., 2017; Pichel et al., 2018a, b), which are
69 particularly relevant for syn-rift salt (Jackson and Hudec, 2017).



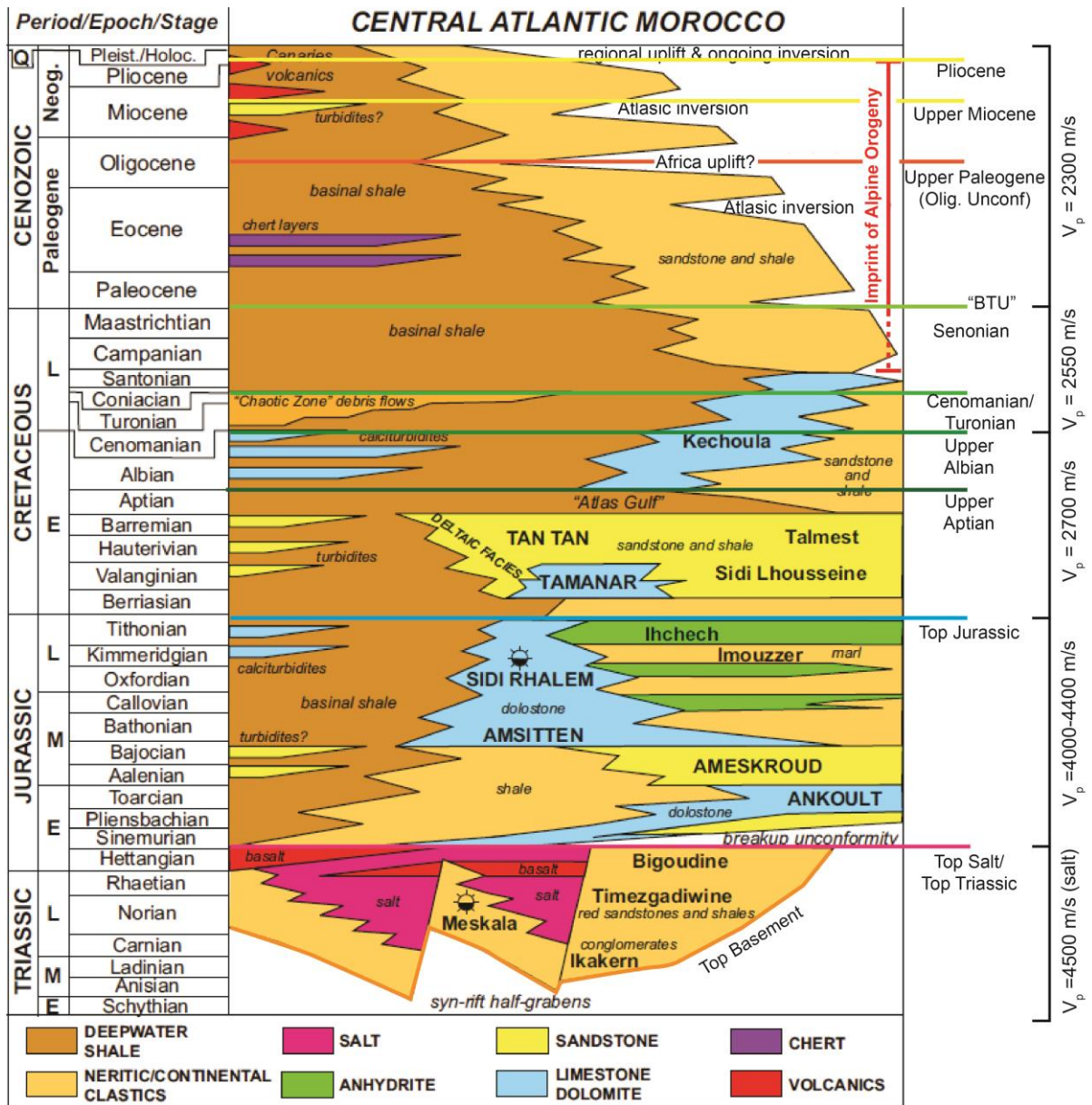
71 *Figure 1: (a) Regional map showing the outline of the Moroccan salt basin and its five main salt-*
72 *related structural domains along the Moroccan margin (adapted from Tari and Jabour, 2013). (b)*
73 *Schematic summary diagram of potential hydrocarbon plays associated with salt structures along*
74 *the margin, most of which remain largely untested (from Tari and Jabour, 2013).*

75 Previous studies provided a regional analysis of salt tectonics offshore Morocco,
76 describing significant along-strike variations in basin geometry and salt-related
77 structures (Fig.1) (Davison 2005; Tari and Jabour, 2013; Tari et al., 2003; 2012). In this
78 study, we expand on them by integrating new seismic (2D and 3D) and well data with
79 both numerical and kinematic models to: 1) test earlier concepts, 2) investigate the
80 mechanisms controlling different salt-related geometries and kinematics along the
81 margin; 3) analyse the effects of base-salt topography and regional tectonic events on
82 salt deformation; and 4) evaluate the timing and generation of allochthonous salt and
83 their potential effects on paleo-bathymetry. The results offer a better comprehension of
84 salt tectonics offshore Morocco, being also relevant for other syn-rift salt basins
85 worldwide. From an applied perspective, this contributes to the regional knowledge of
86 the distribution of potential traps and reservoirs in the deepest and more commercially
87 interesting supra-salt intervals (i.e. Jurassic and Lower Cretaceous, Tari et al., 2012)
88 along the margin.

89 **2. Tectono-stratigraphic framework**

90 The evolution of the Moroccan continental margin started with Triassic rifting
91 associated with opening of the Central Atlantic Ocean and deposition of fluvial red beds
92 and evaporites intercalated with basaltic magma in NNE-SSW to NE-SW half-grabens
93 (Hafid et al., 2000 and 2006, Le Roy and Piqué 2001, Davison 2005; Tari et al., 2003;
94 2012; Tari and Jabour, 2013). A NW-SE syn-rift high, referred to as the Tafelney
95 Accommodation Zone (TAZ), marks a switch in syn-rift fault polarity from NW-dipping

96 faults to the south to SE-dipping faults to the north (Tari and Molnar, 2005; Tari et al.,
 97 2012).



98
 99 *Figure 2: West to East stratigraphic column of Central Atlantic on- and offshore Morocco with the*
 100 *seismic horizons mapped and their respective mean interval velocities highlighted (adapted from*
 101 *Tari and Jabour, 2013). The timing of imprint of Alpine/Atlas orogeny is also annotated.*

102 Break-up and onset of continental drift occurred during the Early Jurassic, with
 103 thermally-induced subsidence and eustatic sea-level rise resulting in marine conditions
 104 and widespread carbonate sedimentation during most of the remaining Jurassic, with
 105 interbedded siliciclastic deposition related to a basin-wide regression (Davison 2005;
 106 Tari et al., 2012; Tari and Jabour, 2013). An Early Cretaceous sea-level rise drowned the

107 carbonate platform and marked a change to siliciclastic sedimentation (Tari et al., 2012;
108 Tari and Jabour, 2013; Luber et al., 2017) (Fig. 2). Carbonate sedimentation returned
109 briefly during the Albian; and throughout the remaining Late Cretaceous and Cenozoic
110 sedimentation was dominated by mudstones and calciturbidites in deep-waters, with
111 apparently very little influx of sands (Tari et al., 2012). The most proximal regions were
112 affected by several episodes of uplift and erosion due to regional compressional
113 tectonics associated with the Atlasic Orogeny, following the collision of Africa with the
114 Iberia Plate and epeirogenic uplift of Africa from the Senonian to recent (Fig. 2) (Hafid
115 et al., 2000; 2006, Davison, 2005; Frizon de Lamotte et al., 2009; Tari and Jabbour,
116 2013). Many authors have argued that thick-skinned compressional events had an
117 influence on the overall structural style of the basin, controlling both onshore (Hafid et
118 al., 2000; 2006, Saura et al., 2014; Vergés et al., 2017) and offshore salt tectonics (Tari
119 et al., 2003; 2012) by progressively tilting the margin and reactivating previous salt
120 bodies.

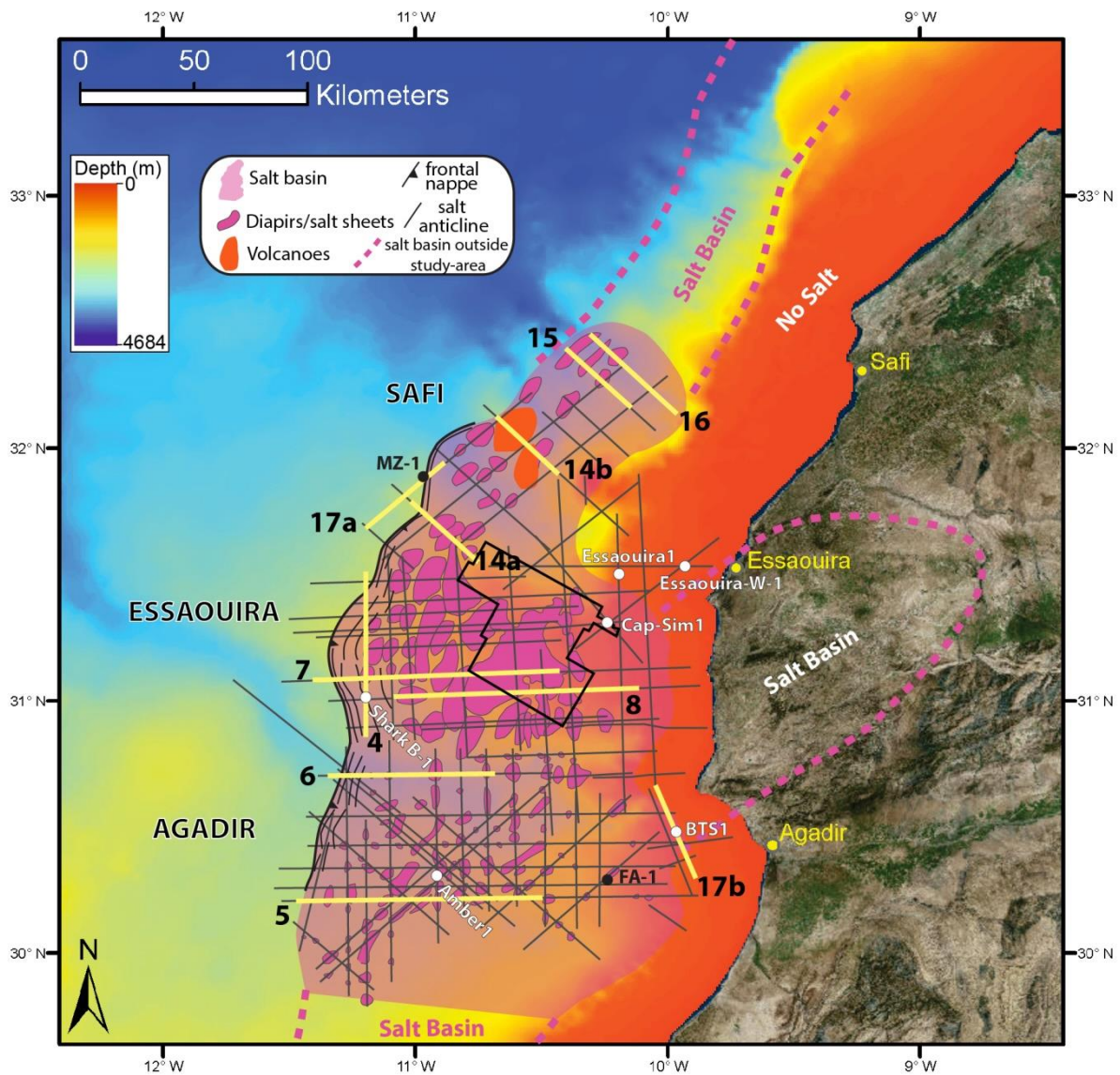
121 Due to the dearth of deep-water wells, the older stratigraphy of the margin is still not
122 well understood, relying on projected information from outcrops onshore Morocco and
123 on Fuerteventura which provide analogues for this deepwater succession (Tari et al.,
124 2012a, b). In Fuerteventura, Jurassic deepwater carbonates directly overly oceanic
125 crust, marking the onset of the drift phase (Aalenian-Bajocian) and being age-equivalent
126 to the prolific carbonate platform inboard (Jansa and Weidman., 1982; Steiner et al.,
127 1998; Davison 2005; Tari et al., 2012). These carbonates are overlain by Jurassic pelagic
128 mudstones, siliclastics turbidites and calciturbidites and Berriasian-Barremian
129 siliciclastics (Tari et al., 2012). Additionally, a series of mass-transport complexes are
130 documented in a seismic-based study (Dunlap et al. 2010), which occur predominantly

131 in the Upper Cretaceous section due to catastrophic failure of the central portion of the
132 margin in the Essaouira Basin.

133 **3. Methods**

134 This study is based on integration of zero-phase, time-migrated 2D regional seismic
135 profiles and 3D seismic data covering c. 2500 km² offshore the Essaouira-Agadir Basin
136 with six offshore wells and numerical models to analyse the salt tectonics along the
137 margin (Fig. 3). Seismic displays follow the Society of Economic Geologists (SEG) normal
138 polarity, where an increase in acoustic impedance with depth is represented by a
139 positive reflection event (red on seismic sections) and a decrease in acoustic impedance
140 by a negative event (blue on seismic sections) (Brown, 2011). 3D and 2D seismic
141 profiles are from different surveys, having variable frequency and resolution. The
142 dominant frequency for the Jurassic varies between 22-28Hz, for the Lower and Upper
143 Cretaceous, it varies between 30-35 and 35-38 Hz respectively; and between 40-50 Hz
144 for the Cenozoic. Based on calibration with sonic-logs from well-ties, the mean interval
145 velocities for these successions are around 2300 m/s for the Cenozoic, 2550 m/s and
146 2700 m/s for the Upper and Lower Cretaceous respectively. As the Jurassic was only
147 penetrated by two wells on the shelf (Essaouira 1 and Essaouira W-1, fig. 3), estimates
148 of deep-water facies velocities are less certain. However, as the Jurassic consists of a
149 carbonate-dominated succession on the shelf (Hafid, 2000; 2006; Hafid et al., 2000; Tari
150 et al., 2012), we infer a marl-dominated slope and deep-basin section, with velocities
151 ranging from 4000-4400 m/s. These values yield an approximate range of vertical
152 resolution of 12-15 m for the Cenozoic, 16-18 m for Upper Cretaceous, 19-22 m for the
153 Lower Cretaceous and of 36-50 m for the Jurassic. The interpretation of key
154 stratigraphic horizons is based on calibration to two deepwater wells (Shark B-01 and

155 Amber 01) and four wells at the shelf (Essaouira 1, Essaouira W-1, Cap Sim 01 and BTS-
 156 01), seismic facies and structural pattern correlations (Fig. 4).



157
 158 *Figure 3: Study-area map with outline of salt basin and main salt structures overlying the present-*
 159 *day bathymetry. The study focuses on three salt provinces that are, from south to north: Agadir,*
 160 *Essaouira and Safi. 2D seismic sections are represented by grey lines, wells in white (used in this*
 161 *study) and black (not available) dots, and outline of 3D survey in the black polygon. Seismic*
 162 *profiles presented in this study are in yellow and numbered according to their respective figure.*
 163 *Onshore satellite image from the ArcMap Online World Imagery layer and the bathymetry from*
 164 *the General Bathymetric Chart of the Oceans (cf. Weatherall et al., 2015).*

165 **4. Results**

166 **4.1. Seismic facies and geometry of key stratigraphic intervals**

167 The Jurassic is characterized by a lower section dominated by moderate amplitude and
168 moderate- to low continuity reflections with occasional, local high amplitude events,
169 passing upwards to moderate- to high continuity, low amplitude reflections (Fig. 4). It
170 displays marked thickness variations across the basin, suggesting strong control on
171 accommodation by salt movement (Figs. 4-8). Its base is defined by a transition from
172 broadly parallel and continuous reflections within the Jurassic to chaotic or wedge
173 shaped intervals that represent basement and Triassic syn-rift strata respectively (Fig.
174 4). The top Jurassic is defined by a high-amplitude positive event that is interpreted to
175 mark the transition from a carbonate-rich section to deep-water clastics of Lower
176 Cretaceous age (Fig. 4) (Tari et al., 2012; Tari et al., 2017).

177 The Lower Cretaceous (Barremian-Aptian, fig. 4) is characterized by moderate- to high
178 continuity and moderate amplitude reflections, transitioning upward to a low amplitude
179 and high-continuity interval delimited at the top by a high-amplitude positive event. The
180 oldest interval penetrated by deep-water wells in the study area (Shark B-1, Cap-Sim 1
181 and Amber 1, figs. 3-4) is Albian in age (Tari et al., 2012), although more recent wells
182 outside the area or not available in this study are reported to have penetrated Aptian
183 (FA-1), Jurassic and possibly Triassic deep-water successions (FD-1 and MZ-1) (W.
184 Leslie, pers. comm. 2018). The Albian interval is broadly isopachous over most of the
185 basin, suggesting a period of decreased salt movement, being dominantly represented
186 by low amplitude and low-continuity seismic facies (Fig. 4). This interval is defined at
187 the top by a positive bright event with moderate continuity that marks an abrupt
188 change to mass-transport complexes characteristic of the Cenomanian (MTCs, Fig. 4)
189 (Dunlap et al., 2010). The Cenomanian presents profound thickness variations and
190 multiple local unconformities over most of the study area (central and northern

191 segments), being characterized by chaotic- to low continuity seismic facies with
192 intermediate high-amplitude and moderate continuity events (Fig. 4). Its top is defined
193 by a moderate- to high amplitude positive event and a transition to highly continuous,
194 moderate- to high amplitude reflections of the remaining Upper Cretaceous, herein
195 referred to as Senonian for simplicity (Fig. 4) (c.f. Tari and Jabour, 2013; Tari et al.,
196 2017).

197 The transition to the Cenozoic is marked by a regional erosional unconformity, the Base
198 Cenozoic Unconformity, also known in the literature as the Base Tertiary Unconformity
199 (BTU, Neumaier et al., 2016) (Fig. 4), which is overlain by highly continuous and
200 variable amplitude facies of Paleogene age. This interval also displays prominent
201 thickness variations and a number of local unconformities can be determined. The top
202 of this interval is defined by an Early Oligocene unconformity (Fig. 4). The remaining
203 Cenozoic is also marked by profound thickness changes intercalated with almost
204 isopachous intervals, both of which display high-moderate amplitude and high-
205 continuity seismic facies. Middle Miocene and Middle Pliocene unconformities mark
206 renewed pulses of regional tectonics linked to the Atlas Orogeny (Tari et al., 2012;
207 2017).

208 Autochthonous and allochthonous salt intervals were defined mainly based on
209 geometries and lateral and/or vertical transition from layered, highly reflective
210 intervals, interpreted to be bedded clastic or carbonate sediments, to chaotic-
211 transparent facies associated with salt. Gently- to moderately-dipping allochthonous
212 top-salt was generally identified as a positive (red) bright event, especially when in
213 contact with the Upper Cretaceous-Cenozoic succession and base-salt as a negative

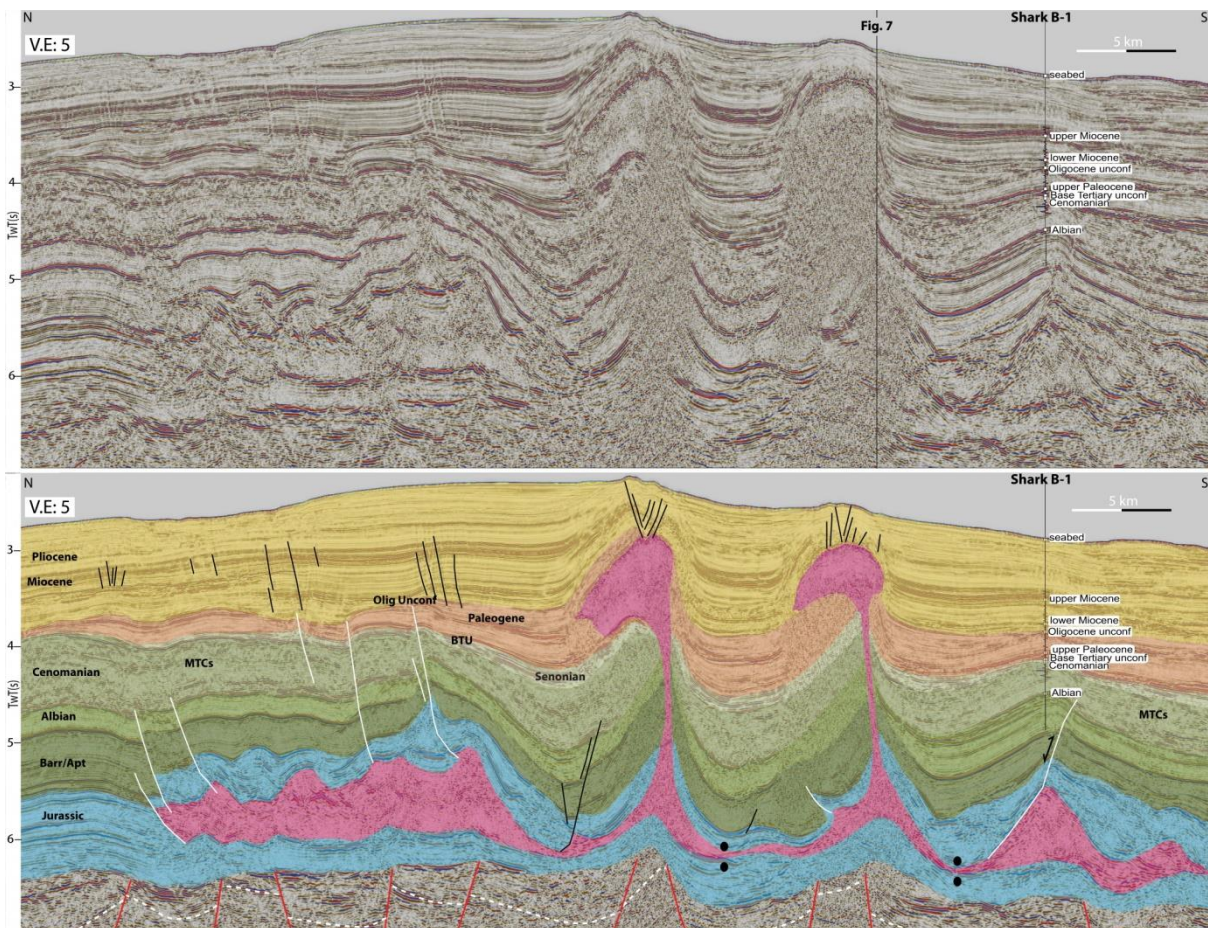
214 (blue) event (Figs. 4-7). The amplitude of these horizons, however, varies considerably
215 according to the juxtaposed units.

216 The Identification of feeders associated with allochthonous salt was based primarily on
217 the interpretation of higher resolution 3D seismic data and generation of structure
218 maps of base and top allochthonous canopy. The presence of feeders in cross-section is
219 then inferred based on the identification of truncations and abrupt lateral changes in
220 geometry aligned with base-allochthonous-salt lows and top-autochthonous-salt highs
221 (Figs. 4-9). In cases where feeders are dipping more gently, they are defined by bright,
222 variably-dipping positive reflections that increase confidence of their interpretation
223 (Figs. 7-9). The identification of feeders allowed recognition of individual allochthonous
224 salt sheets that merged to form large canopies (Figs. 7-9). This was coupled with the
225 chronostratigraphic framework obtained from well-seismic ties and mapping of key
226 horizons (Fig. 4) to provide improved estimates on the timing and mechanisms of
227 emplacement of allochthonous salt along the margin. The timing of emplacement was
228 defined by reasonably confident age estimates of the youngest strata underlying the salt
229 sheets.

230 The base Triassic could be defined locally and is characterised by downwards and/or
231 lateral abrupt transitions from gently-dipping, moderately continuous seismic facies
232 that define typical syn-rift wedge intervals, to chaotic/transparent facies below,
233 interpreted to be high-velocity basement. This observation provided local constraints of
234 syn-rift geometries and allowed identification of basement faults in areas where
235 imaging is less affected by large volumes of salt (Fig. 4-6).

236 Correlation of Mesozoic-Cenozoic intervals across the complex salt structures and
237 minibasins is challenging in parts of the dataset, especially for the deeper and

238 consequently lower resolution intervals, and sections below thick allochthonous salt
 239 (Figs. 4-8). Nevertheless, interpretation in areas of higher confidence could be extended
 240 out- and/or inboard of the salt basin and areas with stronger imprint of salt movement.
 241 This was performed by initially following seismic and structural trends of the main
 242 reflections within minibasins and identifying seismic artefacts related to multiples and
 243 velocity pull-ups (Jones and Davison, 2014); and, subsequently, estimating ages based
 244 on regional analysis and thickness patterns (Figs. 4-6). Nonetheless, a degree of
 245 uncertainty exists for the deeper (Jurassic-Albian) and, therefore, more deformed
 246 intervals in areas far from wells and/or below allochthonous salt sheets.



247
 248 *Figure 4: Uninterpreted and interpreted strike-oriented seismic section over the downdip edge of*
 249 *the salt basin offshore Essaouira and deep-water Shark B-1 well penetrating Upper Albian interval*
 250 *at the crest of a salt-cored anticline (Tari et al., 2012a). This anticline formed by a combination of*
 251 *extension and inversion over the salt nappe. Sub-vertical squeezed feeders associated with inflated*
 252 *salt tongues having minor sea-floor expression are interpreted not to be welded due to current*
 253 *activity and uplift of a thick overburden. The section also shows folding and thrusting related to*

254 *advance of salt nappe over syn-kinematic Jurassic sediments and a zone of folding and uplift north*
255 *of the salt basin associated with thick-skinned contraction. Uninterpreted section exemplifies the*
256 *main seismic facies associated with main stratigraphic interval interpreted in this study. Vertical*
257 *Exaggeration is c. 5-fold based on an average velocity of 4000m/s.*

258 **4.2. Salt-related structures and along-strike variation across the margin**

259 The Moroccan Atlantic margin is characterized by a complex pattern of salt walls,
260 diapirs and allochthonous salt sheets with prominent along-strike variation (Tari et al.,
261 2003; 2012; 2017; Tari and Jabour, 2013) comparable to its conjugate margin in Nova
262 Scotia (Ings and Shimeld, 2006; Albertz et al., 2010; Deptuck and Kendell, 2017). Five
263 different salt tectonics domains were defined by Tari et al. (2012) and Tari and Jabour
264 (2013) (Fig.1).

265 The southernmost, Segment I (Cap Juby area), is characterized by few and simple
266 structures represented by salt pillows and up-right diapiric salt walls, downdip of the
267 large Jurassic shelf (Fig. 1). Northwards, Segment II (Tarfaya and Agadir Basins),
268 comprises a large number of salt walls and stocks, a few of which are associated with
269 minor salt tongues and are described as being mainly driven by sedimentary loading
270 during the Cenozoic (Tari et al., 2003; 2012; Tari and Jabour 2013) (Fig. 1a). The north
271 of Segment II (Tafelney Plateau, Essaouira Basin) is defined as the salt-richest portion of
272 the margin with a larger number of structures and most complex salt tectonics
273 characterized by allochthonous salt sheets and an outboard salt nappe and fold-thrust
274 belt (Tari and Jabour, 2013). Segment III (Safi) contains fewer salt structures and only
275 small (c. 10-20 km²) allochthonous salt bodies, probably due to a smaller original
276 volume of salt (Tari et al., 2012). The northernmost segments contain simpler salt
277 tectonic styles, characterized by a large number of diapirs in Segment IV, with a few
278 long (c. 100 km) salt walls in Segment V (Fig 1a) (Tari et al., 2012; Tari and Jabour,
279 2013).

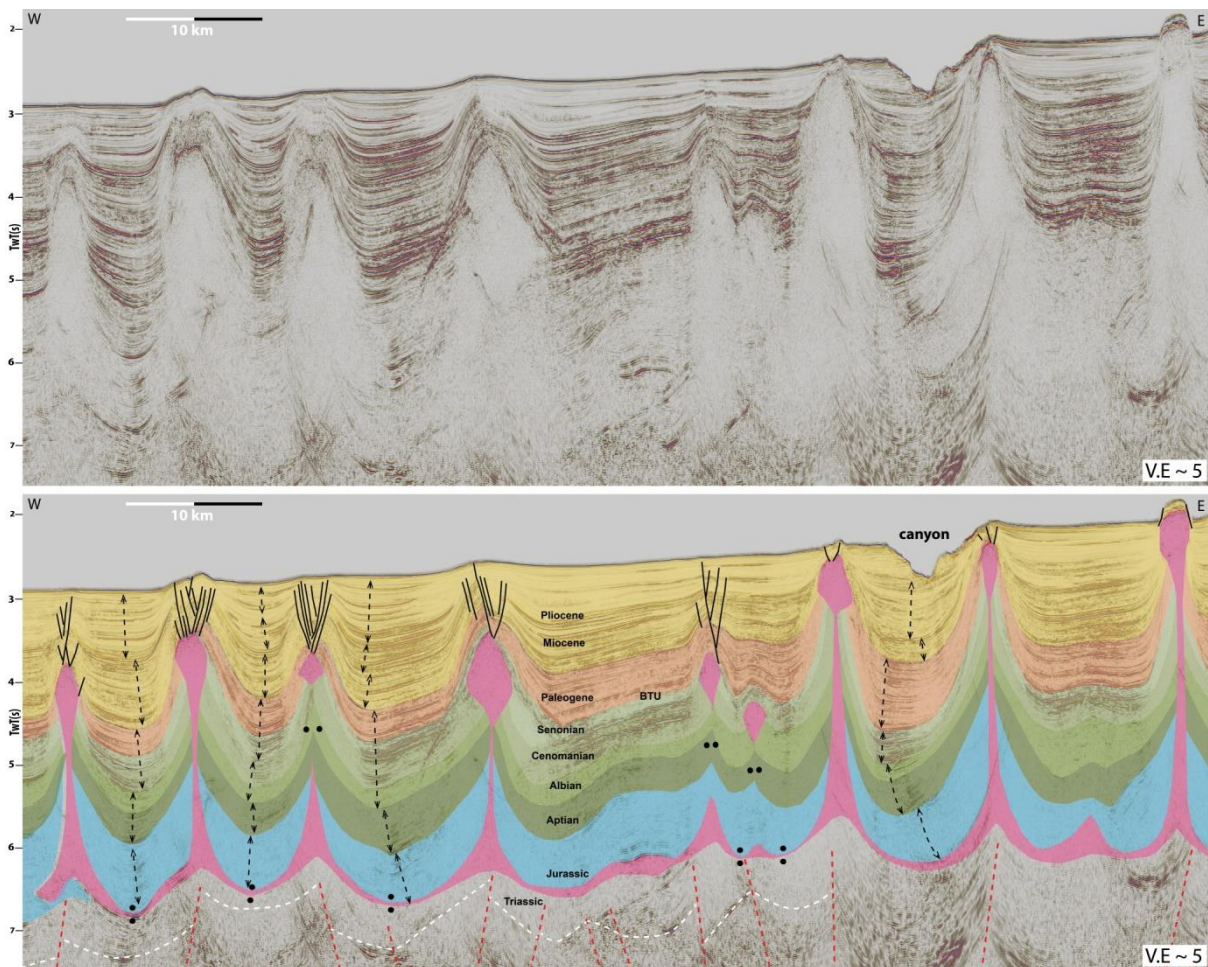
280 Similar to the conjugate margin (Adam and Krézsek, 2012; Deptuck and Kendell, 2017),
281 the syn-rift nature of the salt has been demonstrated to be an important factor on the
282 evolution of Atlantic Morocco, controlling original along-strike thickness variations
283 (salt-rich and salt-poor segments, c.f. Tari et al., 2003; 2012; Tari and Jabour, 2013) and
284 also limiting salt-detached translation (Tari and Jabour, 2013). Nonetheless, the effects
285 of pre-salt rift topography and associated salt thickness variations on supra-salt
286 kinematics and structural styles; combined with the influence of margin configuration,
287 base-salt relief and late tectonic events on the generation of allochthonous salt along the
288 margin have not yet been addressed in detail. This paper, therefore, focuses on
289 segments II-III of the original division of Tari et al. (2012) (Fig. 1), subdividing them into
290 3 segments: the (1) Agadir; (2) Essaouira and (3) Safi Basins (Fig. 3) to investigate these
291 issues.

292 **4.2.1. Agadir Basin**

293 This segment has the thickest overburden at c. 7 km, and deepest autochthonous salt (c.
294 9-10 km depth below sea surface) of the entire study-area (Fig. 5). The area is
295 characterized by tall (c. 4-6km), up-right diapirs with thin (< 400 m wide) to welded
296 sub-vertical stems and, predominantly, broadly symmetric salt bulbs up to 2 km wide,
297 defining classic tear-drop diapirs (Fig. 5). Despite the 2D nature of the dataset in this
298 segment, certain structures can be followed in multiple sections along-strike and are
299 characterized as 5-10 km long walls trending predominantly NE-SW. The majority of
300 diapirs, however, can be described as salt stocks having an axial ratio of less than two
301 (c.f. Jackson and Hudec, 2017) (Fig. 3).

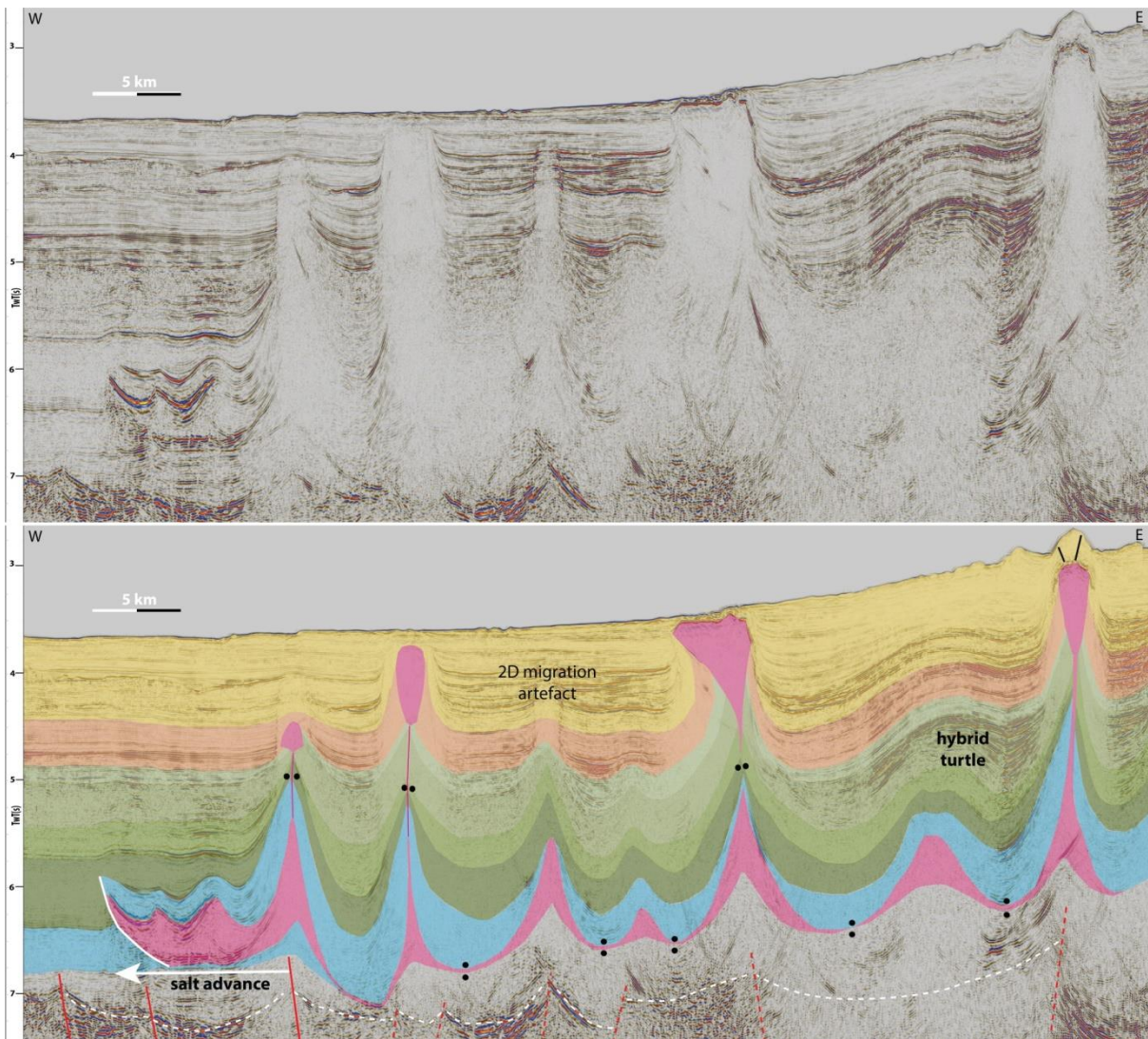
302 These diapirs are surrounded by 5-10 km wide minibasins, 3-7 km thick, that are
303 apparently welded or occur above thin (c. 200 m) autochthonous salt (Fig. 5). These

304 minibasins exhibit pronounced thickness variations in the Middle Jurassic to Early
 305 Cretaceous interval, which are directly and often abruptly truncated against the diapiric
 306 stems. This indicates early passive rise driven by differential sedimentary loading and
 307 salt expulsion below subsiding minibasins (*sensu* Hudec et al., 2009, Peel 2014a). Some
 308 of the Jurassic-Lower Cretaceous depocentres present landward-dipping depositional
 309 axial traces (dashed black line, fig. 5) that may indicate an early phase of expulsion
 310 rollover. A brief precursor phase of reactive rise is likely to have occurred in the Early-
 311 Middle Jurassic, as salt had been deposited at the end of the rift stage and, thus, syn-
 312 extension (*sensu* Rowan 2014; Jackson and Hudec, 2017), but this is overprinted by a
 313 long-lived, multiphase growth (Tari and Jabour, 2013; Tari et al., 2017).



314
 315 *Figure 5: Uninterpreted and interpreted regional seismic section at the southern portion of Agadir*
 316 *Basin showing tall, up-right, highly-squeezed and broadly symmetric diapirs, some of which*
 317 *forming tear-drop structures and others with sea-floor expression. Minibasins present strong*

318 thickness variations from Jurassic-Lower Cretaceous and Paleogene-Miocene indicating the main
 319 period of growth, mostly associated with regional shortening as evidenced by abrupt shift of
 320 depocentres (black dashed lines). Sub-salt dashed-lines are used for faults (red) and the base-
 321 Triassic horizon (white), which are subject to uncertainties due to typical sub-salt imaging issues
 322 but can be inferred based on a combination of supra-salt geometries and sub-salt seismic facies
 323 variations and truncations. Two types of faults occur at the crest of diapirs, keystone and flap
 324 faults (c.f. Jackson et al., 1999), which indicate outer-arc extension, roof uplift and contraction
 325 during the Cenozoic. Vertical Exaggeration is c. 5-fold based on an average velocity of 4000m/s.



326
 327 Figure 6: Uninterpreted and interpreted regional seismic section north of Agadir, near transition
 328 to Essaouira showing a 8 km wide salt nappe recording frontal advance, passing updip to up-right
 329 tear-drop to a sub-vertical squeezed feeder and inflated salt tongue and another up-right squeezed
 330 diapir with sea-floor expression further updip. Hybrid turtle anticline forms between the latter due
 331 to a combination of salt subsidence and translation over a large pre-salt graben. Sub-salt dashed-
 332 lines are used for faults (red) and the base-Triassic horizon (white), which are subject to
 333 uncertainties due to typical sub-salt imaging issues but can be inferred based on a combination of
 334 supra-salt geometries and sub-salt seismic facies variations and truncations. Vertical Exaggeration
 335 is c. 5-fold based on an average velocity of 4000m/s.

336 Thickness variations within minibasins and, consequently, the record of salt activity
337 generally decrease during the Albian-Cenomanian and most diapirs become partially
338 buried by Senonian-Paleocene strata (Figs. 5-6). The diapirs, however, push and uplift a
339 relatively thick (up to 1.5 km), isopachous roof that is overlapped by Miocene-Pliocene
340 strata exhibiting significant thickness variations and indicating diapirism was
341 rejuvenated by renewed pulses of active rise during this time (Fig. 5). Keystone and flap
342 faults (*sensu* Rowan et al., 1999) develop at their crests due to outer-arc extension and,
343 combined with sub-vertical squeezed stems and abrupt shifts of the depositional axial-
344 traces within minibasins (Fig. 5), indicate that active rise was driven by shortening. The
345 smaller tear-drop diapirs become dormant by the Pliocene, but most structures present
346 sea-floor expression denoting ongoing activity (Figs. 5-6).

347 In the southernmost portion of this segment, the absence of a salt nappe at the frontal
348 edge of the salt basin and the predominantly vertical salt structures suggest no
349 significant basinward translation (Fig. 5). Salt and overburden translation due to
350 basinward gliding increase progressively northwards towards Essaouira, but is
351 relatively minor (< 10 km) as shown by the appearance of a 5-9 km wide, c. 1.5 km
352 thick, sub-horizontal salt nappe and symmetric fold-belt at its northern limit with the
353 Essaouira segment (Fig. 6). Diapir spacing is c. 8-10 km downdip, and most diapirs,
354 especially the largest of them, appear to be, at present, above or near the footwall crest
355 of syn-rift faults in areas where faults can be estimated (Figs. 5-6).

356 **4.2.2. Essaouira Basin**

357 The central segment, the offshore Essaouira Basin, also referred as Tafelney Plateau (c.f.
358 Tari and Jabour, 2013), has a strikingly different structural style, being characterized by
359 a large number of allochthonous salt bodies, seaward-verging diapirs and salt tongues

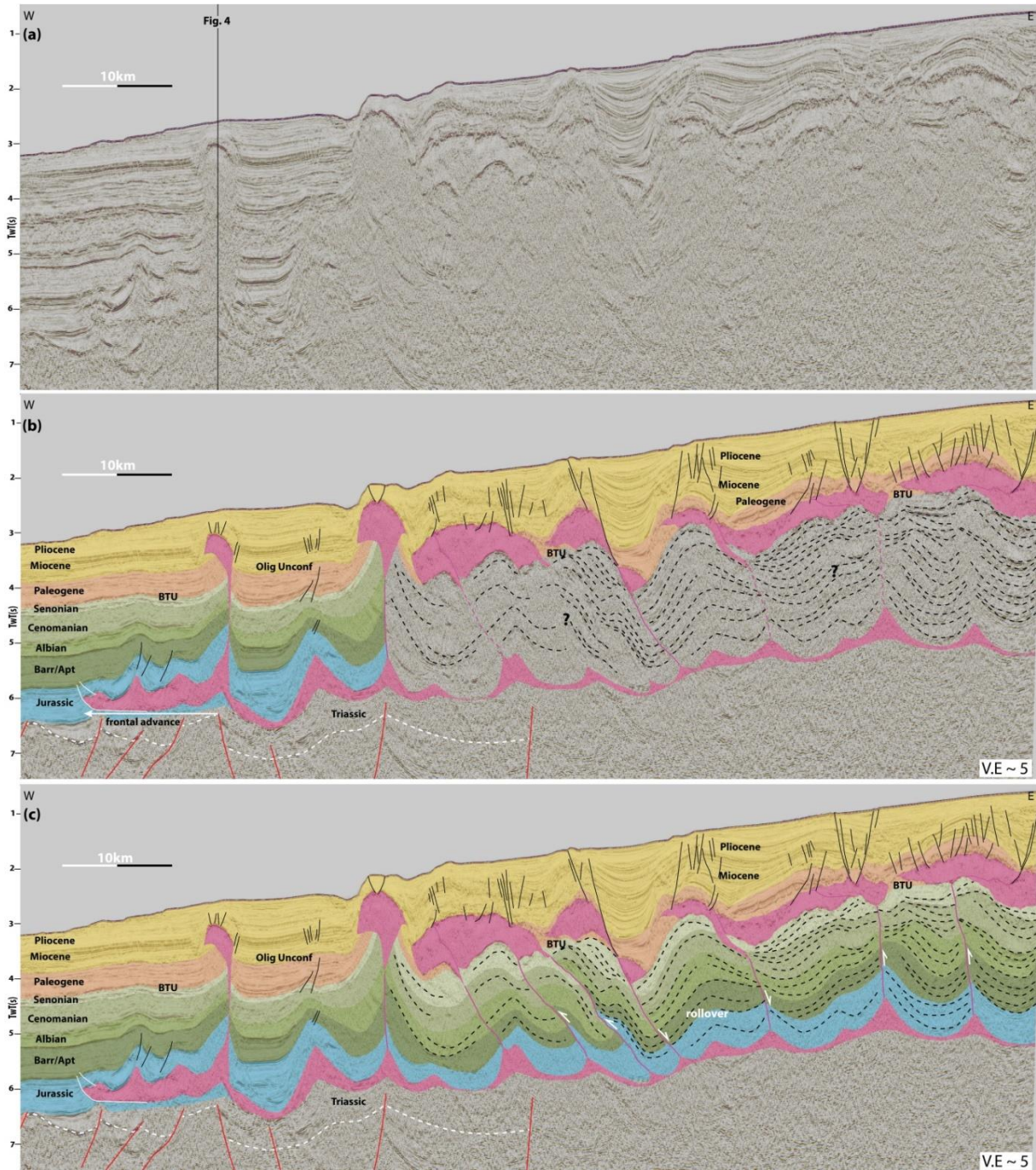
360 (Figs. 7-8) (Tari et al., 2000; 2003; 2012; 2017). This segment is also defined by a
361 prominent downdip salt nappe and fold-thrust belt (Tari and Jabour, 2013) recording
362 the highest magnitude (c. 14-20 km) and rate of salt and overburden translation in the
363 entire margin (Figs. 3-7). The magnitude is estimated based on the distance from the
364 frontal edge of the nappe to the original limit of the salt basin, which coincides with a
365 large landward-dipping pre-salt fault (Fig. 7). Middle Jurassic-Aptian growth synclines
366 are capped by a broadly isopachous Albian interval in the salt-cored fold-belt over the
367 nappe suggesting translation occurred during that period and, therefore, at c. 0.2-0.4
368 km/Ma (Fig. 7). Although within the range of salt-flow rates described for passive
369 margins (Rowan et al., 2004; Peel 2014b), these values are generally lower than flow
370 rates reported for post-rift salt basins (up to 0.8 km/Ma) such as Angola and Brazil
371 (Peel 2014b; Pichel et al., 2018a).

372 3D data images the largest salt canopy in the basin together with a number of other
373 smaller allochthonous sheets (Figs. 3 and 9-13). TWT structure maps of the top and
374 base-allochthonous salt (Fig. 9a-b) show a canopy with an area of 1390 km², maximum
375 thickness of c. 2.7- 2.9 km and average thickness of 1.2 km (Fig. 9c). The identification
376 of semi-circular lows at base- and top-canopy levels (Fig. 9a-b) aligned with steep
377 seaward-leaning sub-salt truncations and salt pedestals at the autochthonous level in
378 cross-section (Figs. 8 and 10-12), permitted confident interpretation of at least five
379 individual feeders (Fig. 9). These feeders indicate that the canopy formed by the
380 coalescence of a minimum of five smaller salt sheets due to early downdip gliding and
381 spreading.

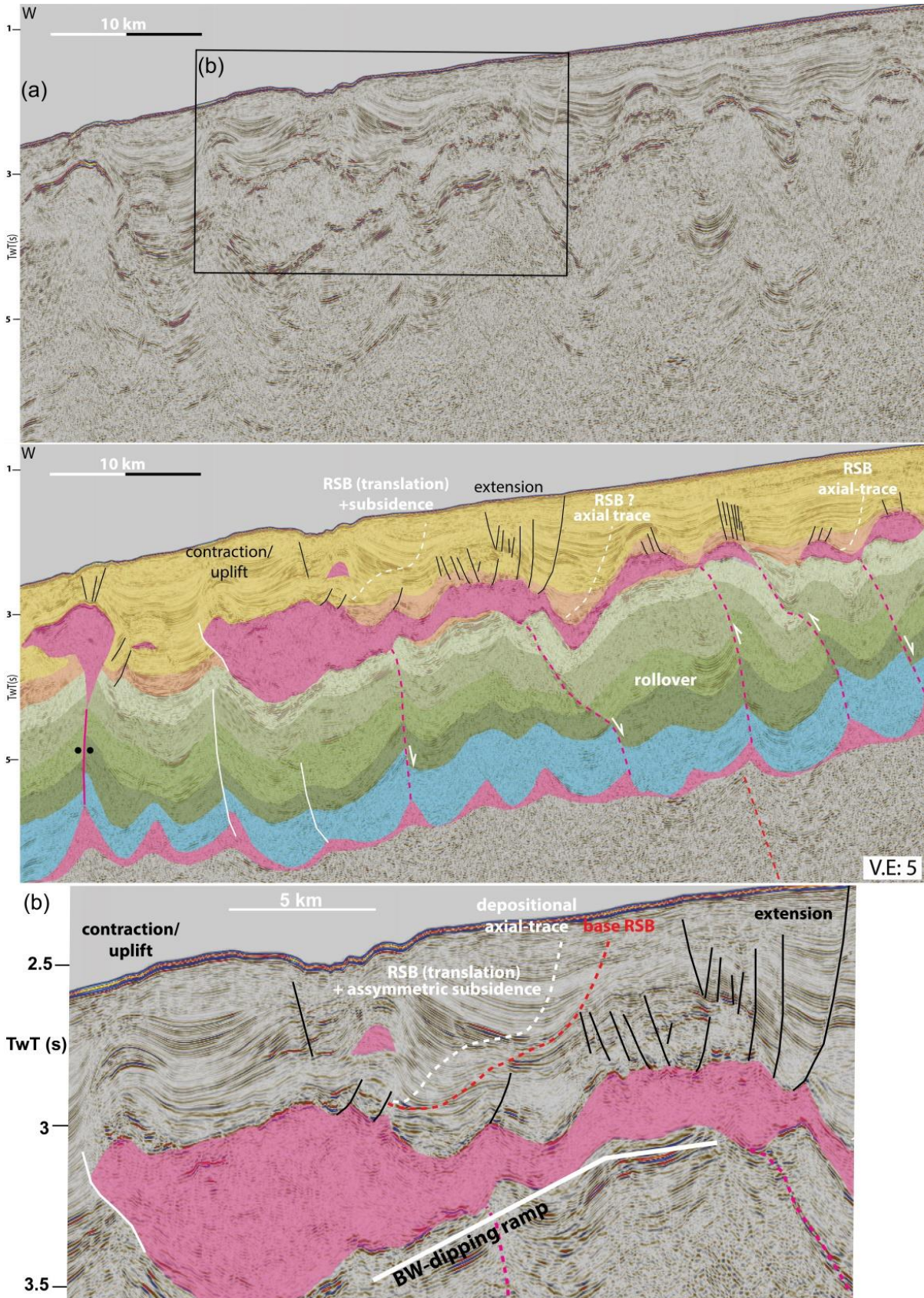
382 The recognition of individual sheets and their associated feeders permitted
383 interpretation of the kinematics and growth patterns in various sub-salt minibasins. The

384 allochthonous salt sheets are linked to the autochthonous level by predominantly
385 counter-regional (*sensu* Schuster, 1995), seaward-verging and apparently-welded
386 feeders associated with variable geometries and growth strata (Figs. 7-13). They can be
387 associated with expulsion and/or extensional rollovers (c.f. Ge et al., 1997; Krezsec et
388 al., 2007; Jackson et al., 2015a) where hangingwall strata dip gently basinward and
389 thicken towards the feeders, subsiding relative to its footwall further downdip (Figs. 7-
390 8). Their hangingwalls can also dip dominantly landward and sub-parallel to the feeders
391 showing a reverse sense of movement relative to the footwall, thinning towards the
392 feeders and fold-geometries suggestive of thrust-related folding (c.f. Shaw et al., 2005;
393 McClay et al. 2011) and contraction (Figs. 7-8, 10 and 12-13).

394 These variations indicate an early evolution and emplacement of allochthonous salt
395 linked to at least two different mechanisms: i) extension and/or subsidence of supra-
396 salt strata leading to seaward salt expulsion, and ii) contraction and uplift. These
397 mechanisms alternate downdip and along-strike with zones of uplift and contraction
398 passing downdip to areas of extension and salt expulsion, and further downdip to
399 another zone of contraction (Figs. 7-8a-b, 10 and 12-13). This structural zonation
400 challenges the conventional view of regional gravity-driven salt deformation in passive
401 margins where updip extensional domains are linked to downdip basin edge
402 contractional provinces by a broadly undeformed translational zone (c.f. Rowan et al.,
403 2004; Brun and Fort, 2011; Quirk et al., 2012; Jackson et al, 2015a).



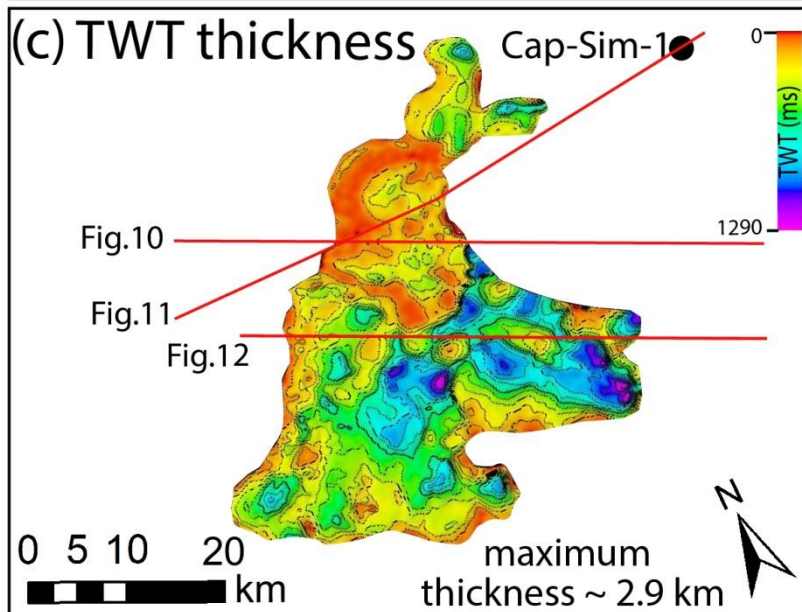
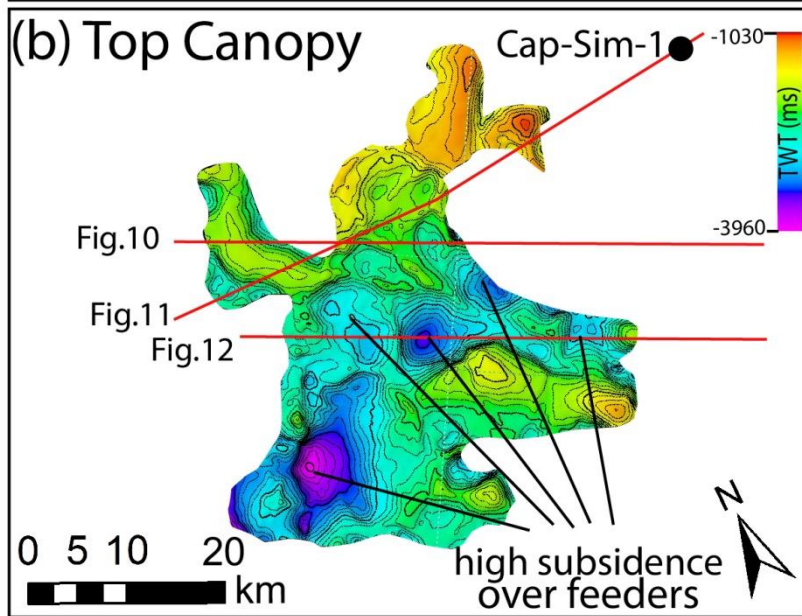
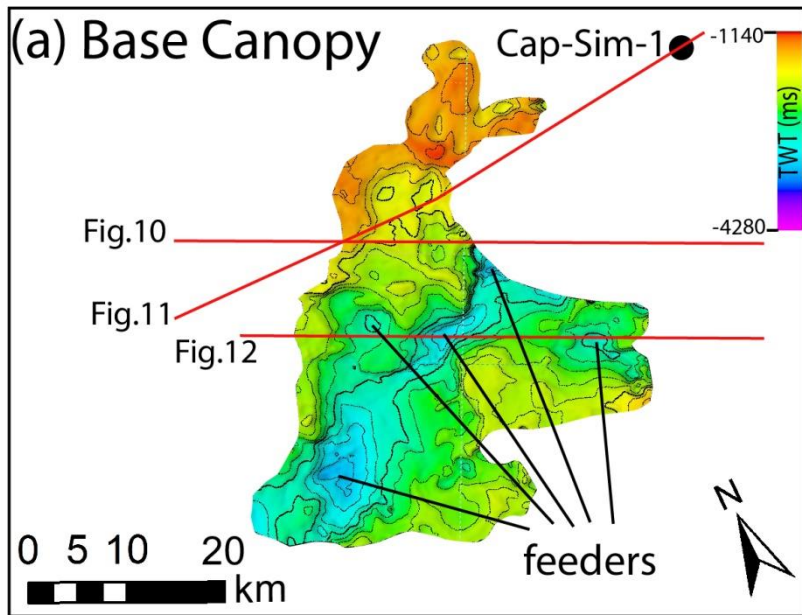
404
 405 *Figure 7: (a) Uninterpreted, (b) semi-interpreted and (c) fully-interpreted regional seismic section*
 406 *offshore Essaouira showing the widespread occurrence of allochthonous salt sheets and canopy fed*
 407 *by sub-vertical to seaward-leaning feeders exhibiting complex kinematics and along-dip*
 408 *alternation of extensional (basinward-dipping rollovers) and contractional provinces (reverse*
 409 *shearing and folding). The downdip end of the basin is characterized by a c. 15 km wide salt nappe*
 410 *and sub-vertical squeezed diapirs with asymmetric salt tongues. Sub-salt dashed-lines are used for*
 411 *faults (red) and the Base-triassic horizon (white), which are subject to uncertainties due to typical*
 412 *sub-salt imaging issues but can be inferred based on a combination of supra-salt geometries and*
 413 *sub-salt seismic facies variations and truncations. The relative displacements of minibasins are*
 414 *indicated by white arrows. Vertical Exaggeration is c. 5-fold based on an average velocity of*
 415 *4000m/s.*



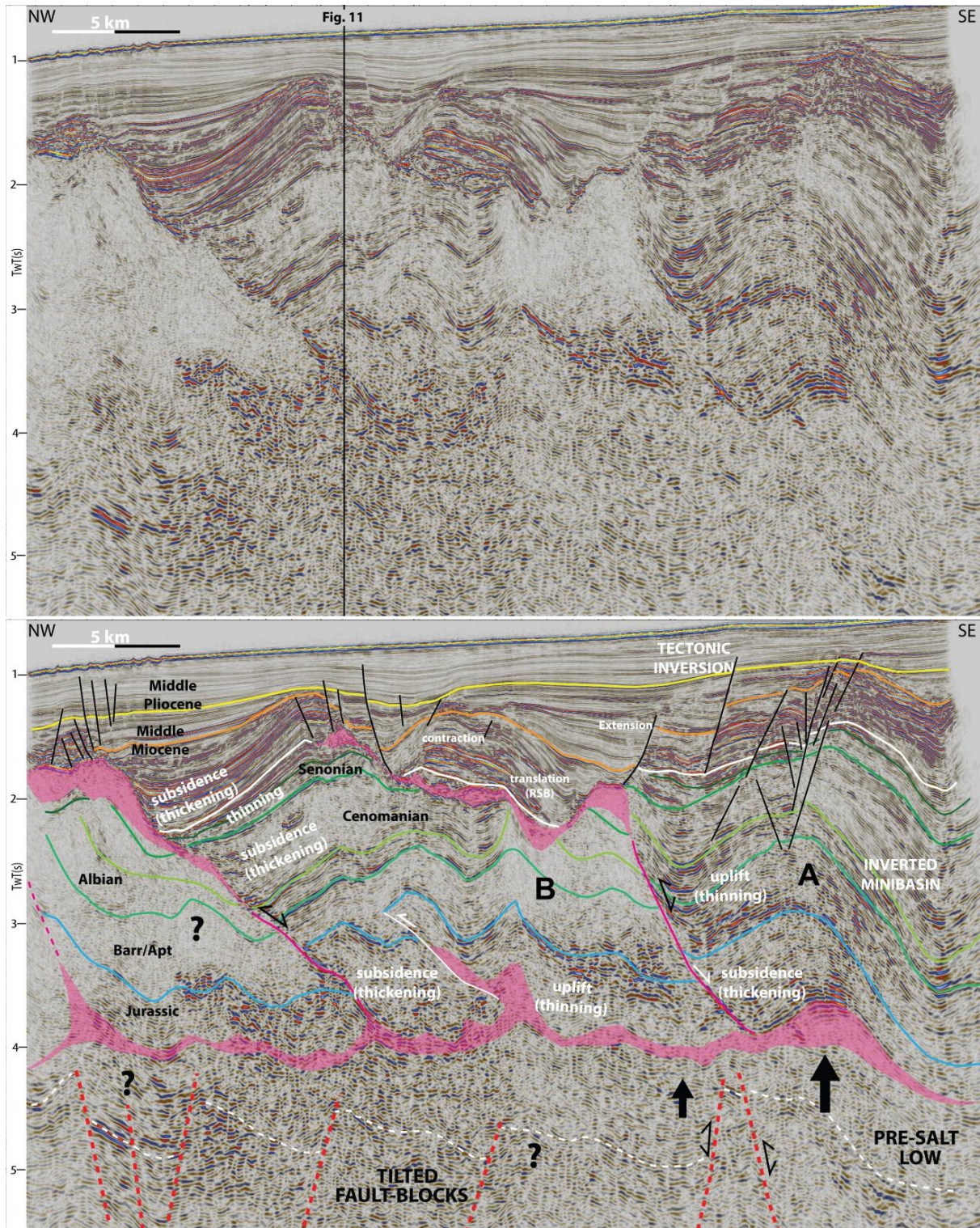
417
 418 *Figure 8: (a) Uninterpreted and interpreted regional seismic section offshore Essaouira showing*
 419 *the widespread occurrence of allochthonous salt sheets and a c. 35 km wide canopy fed by sub-*
 420 *vertical to seaward-leaning feeders exhibiting complex kinematics and along-dip alternation of*

421 *structural styles. Allochthonous salt sheets exhibit updip extension, intermediate landward-*
422 *thickening asymmetric minibasins (i.e. RSBs) formed over basinward-dipping base-salt ramps and*
423 *recording 8 km of translation; passing downdip to zones of uplift and contraction. Zoom in (b).*
424 *Vertical Exaggeration is c. 5-fold based on an average velocity of 4000m/s.*

425 3D seismic data provides a more detailed picture of these complex minibasin
426 geometries, showing that hangingwall strata associated with counter-regional feeders
427 commonly present switches in their kinematics and growth pattern through time (Figs.
428 10-13). The landward minibasin (A, fig. 10) and its seaward-verging salt feeder shows
429 an early history of subsidence and basinward-thickening associated with a Jurassic
430 rollover, followed by stratal thinning and uplift against the same feeder in the Early
431 Cretaceous-Cenomanian indicating lateral contraction and thrusting. The minibasin
432 immediately downdip (B, fig. 10) presents the opposite growth history. Thinning,
433 buckling and thrust-related folding of the Middle Jurassic interval indicates Jurassic
434 contraction and thrust salt-piercement; passing upwards within the same minibasin to
435 Early Cretaceous-Cenomanian basinward subsidence and thickening (Fig. 10). These are
436 gently-dipping in response to the vertical load associated with minibasin subsidence
437 and basinward-thickening strata, and are sub-vertical due to lateral displacement
438 loading related to shortening and diapir squeezing (Figs. 10-11).



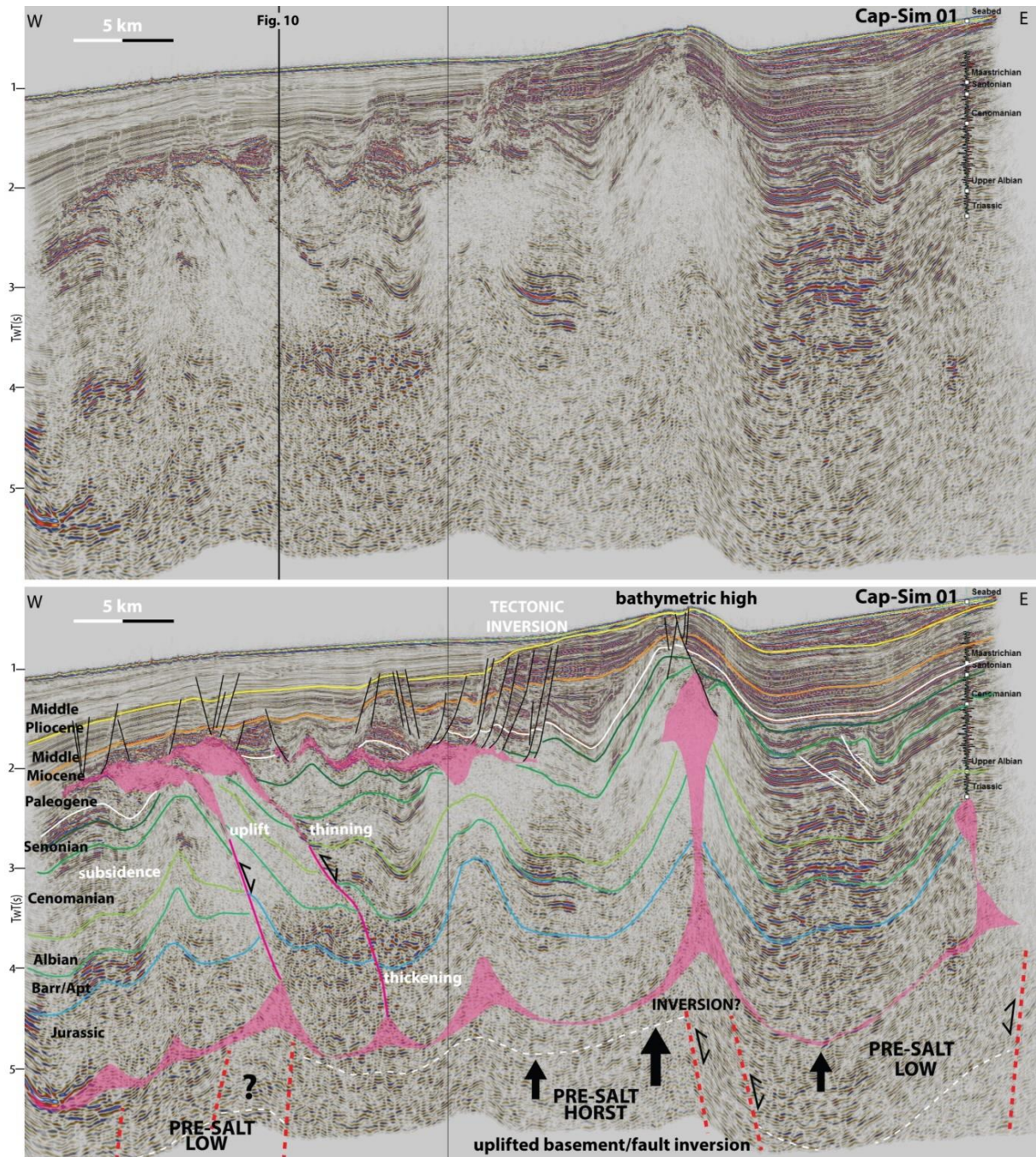
440 Figure 9: (a) base, (b) top and (c) thickness map of allochthonous salt canopy in Essaouira
 441 generated from 3D seismic dataset with the approximate location of 3D seismic sections presented
 442 in figures 10-12. The location of feeders and original smaller sheets are identified by base-salt and
 443 top-salt lows and ramps.



444 Figure 10: Uninterpreted and interpreted 3D seismic section showing complex kinematics on over
 445 both autochthonous and allochthonous salt. Updip minibasin shows Jurassic basinward-thickening
 446 rollover passing upward to thinning Lower Cretaceous section against a seaward-leaning
 447 squeezed feeder that originates a c. 10 km wide salt sheet. The minibasin further downdip shows
 448

449 *the opposite growth history with Jurassic buckle-folding and thrusting indicating contraction*
450 *passing upward to basinward-dipping and thickening Cretaceous section. Both minibasins are then*
451 *inverted and contractionally deformed during the Senonian to Paleogene. These geometries can*
452 *guide estimation of pre-salt structures below (dashed lines). The allochthonous sheet is defined*
453 *updip by basinward-dipping normal faults, intermediate translation (RSB) and uplift passing to a*
454 *zone of counter-regional flow at its landward-dipping downdip edge. Black arrows denote uplift*
455 *related to thick-skinned tectonics and reactivation of pre-salt rift faults, with their size*
456 *quantitatively denoting the magnitude of uplift.*

457 General thinning and uplift of Senonian-Paleogene strata towards squeezed salt stems
458 indicate a regional pulse of contraction and inversion (Figs. 10-13). This coincides with
459 periods of regional thick-skinned contraction both onshore and offshore Morocco (Hafid
460 et al., 2006; Tari and Jabour, 2013), suggesting late minibasin inversion was driven by
461 basement-involved contraction and uplift. A large, 10-15 km wide present-day
462 bathymetric high, cored by a zone of uplifted and possibly inverted basement and with a
463 squeezed diapir at its centre suggests basement-involved inversion is still ongoing and
464 greater north-eastwards in the Essaouira Basin (Fig. 11). Despite poor imaging of the
465 pre-salt interval, the presence of a shallower autochthonous salt at this portion of
466 Essaouira and uplift of a >1km thick roof by the squeezed diapir support an
467 interpretation of basement-involved contraction and inversion of syn-rift faults (Fig.
468 11), as diapirs are typically not capable of uplifting such a thick roof purely by buoyancy
469 (Jackson and Hudec, 2017).



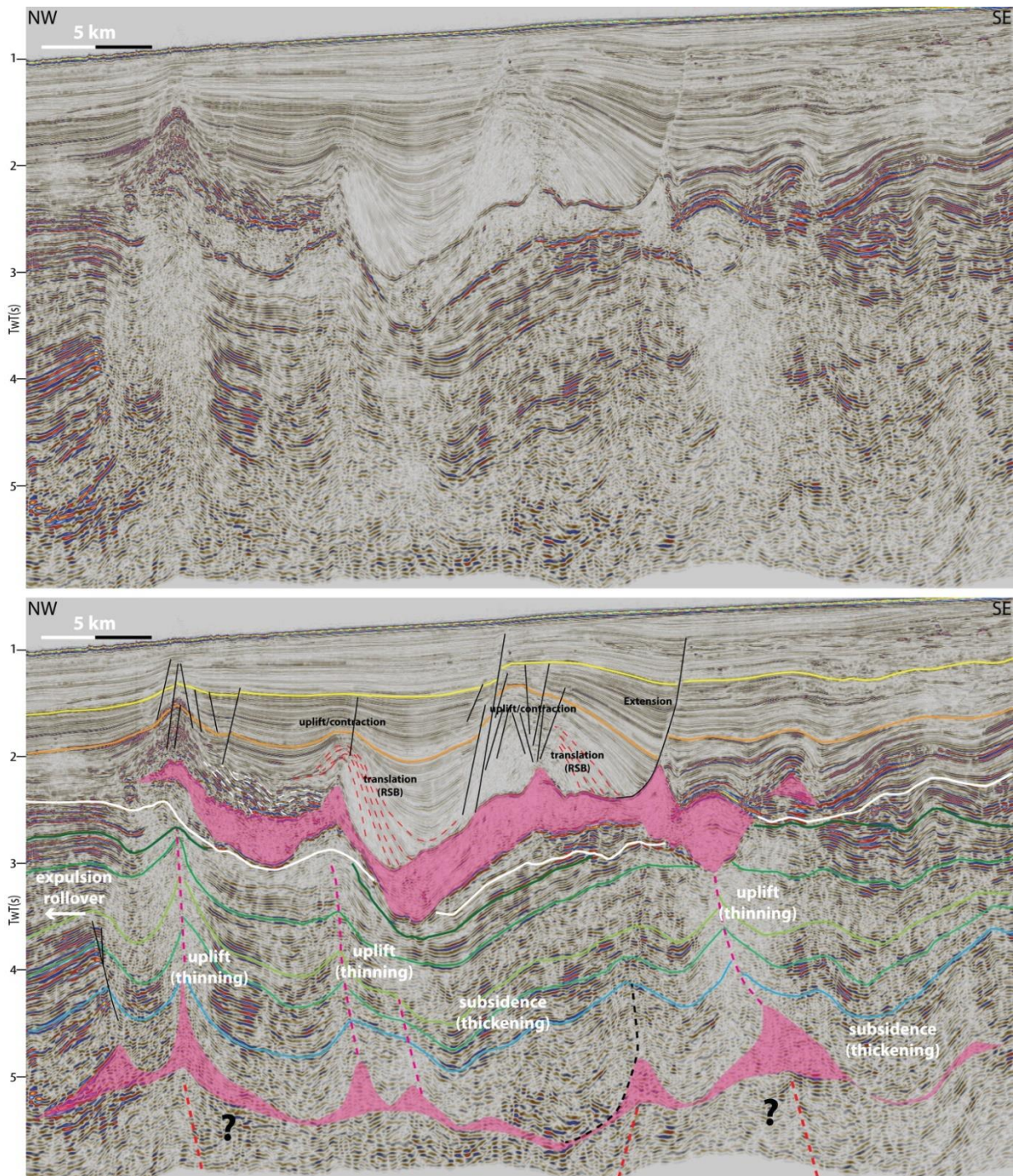
470
 471 *Figure 11: Uninterpreted and interpreted 3D seismic section with Cap-Sim 01 well penetrating*
 472 *Upper Albian and Triassic salt without Aptian and Jurassic section indicating the presence of a*
 473 *diapir. The section illustrates a highly squeezed sub-vertical diapir uplifting a c. 1 km thick roof*
 474 *and generating sea-floor topography. The smaller volume of salt and shallower autochthonous salt*
 475 *allow identification of certain pre-salt rift geometries (dashed lines) that indicate uplift and*
 476 *inversion of syn-rift faults. Further downdip a thin Senonian allochthonous sheet with salt rollers*
 477 *and basinward-dipping normal faults indicates downdip gliding and salt evacuation. Further*
 478 *basinward, two stacked salt sheets nucleate from seaward-leaning feeders over the top-Cretaceous*
 479 *interval. Feeders show complex kinematics and multiphase growth patterns with early basinward-*
 480 *thickening and later basinward-thinning indicating inversion.*

481 At the allochthonous level, salt deformation is characterized by the alternation of
482 kinematically-linked domains of extension, translation and contraction, which indicates
483 basinward movement of salt and overburden and the influence of base-salt relief (Figs.
484 7-8 and 10-13). Updip extension is represented by listric basinward-dipping normal
485 faults and extensional, landward-thickening rollovers (Figs. 5, 7-8). These occasionally
486 define roho-systems (*sensu* Schuster, 1995; Rowan et al., 1999) (updip sheets in figs. 7
487 and 11) and may be associated with small salt rollers and nearly-welded salt due to
488 large basinward salt evacuation (Fig. 11). Contraction is characterized by folding and
489 uplift of roof strata with outer-arc extension (keystone faults) or squeezing and
490 steepening of their landward-dipping frontal edge (Figs. 7-8). The amount of extension
491 is generally greater than the observed contraction, suggesting extension and downdip
492 gliding were initially accommodated by open-toe salt advance (*sensu* Hudec and Jackson
493 2006) as the sheets were emplaced at or near the sea-floor. In wider (> 5 km) sheets
494 and canopies, extension is usually linked to downdip contraction by an intermediate
495 zone of translation where landward-dipping growth strata define Ramp-Syncline Basins
496 (RSBs, c.f. Pichel et al., 2018a). These basins were initially described to form above
497 autochthonous salt by translation over basinward-dipping base-salt ramps (Jackson and
498 Hudec, 2005), and here they develop by movement over similar ramps but at an
499 allochthonous level (Figs. 7-8, 10 and 12-13). These minibasins are strongly
500 asymmetric, being characterized by predominantly landward-thickening sigmoidal
501 strata and a basinward-dipping axial trace (Figs 7-8 and 12-13). They may directly
502 onlap the top of the salt sheet indicating translation started immediately after extrusion
503 (Figs. 10-13); or a thin (c. 100-200 m thick) pre-kinematic cover where the initial
504 translation occurred over a flat surface or, alternatively, started later (Figs. 7-8). They
505 terminate updip above a base-salt basinward-dipping ramp, being occasionally near but

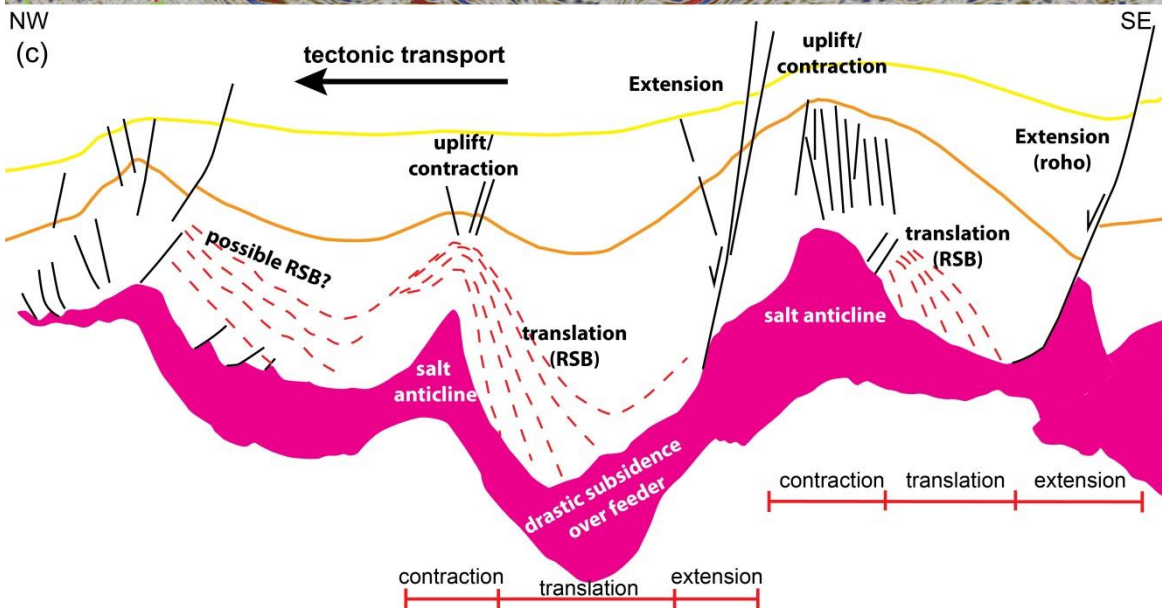
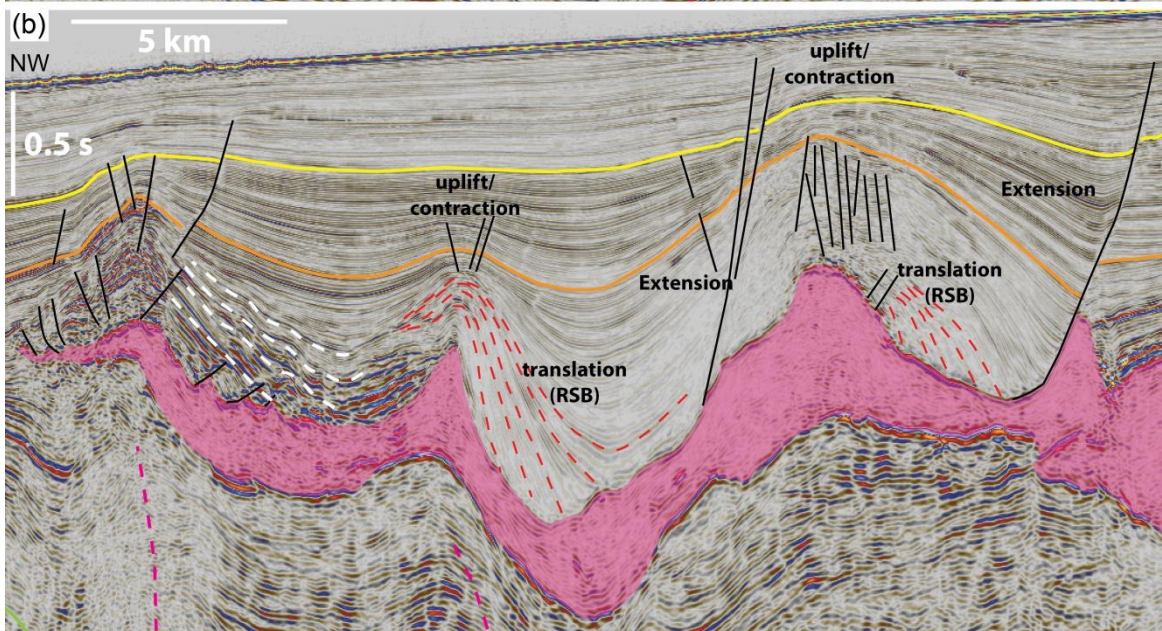
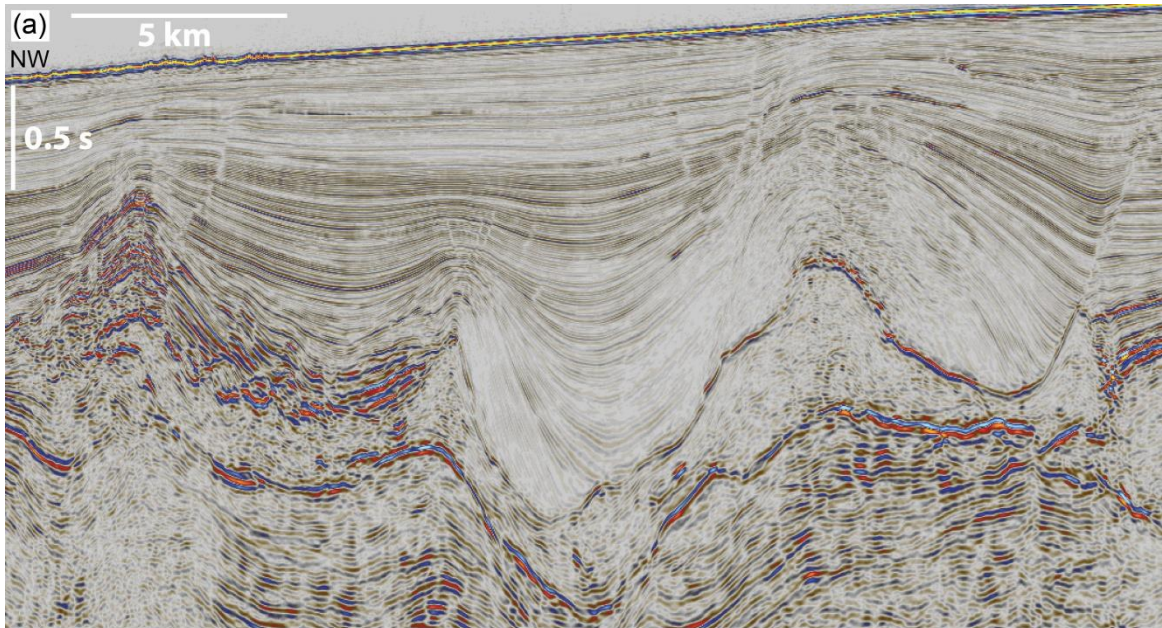
506 not in direct contact with basinward-dipping normal faults (Figs. 7-8 and 10); and in
507 places appear highly rotated and onlapping a steep landward-dipping top-
508 allochthonous salt (Figs. 12-13). These relationships indicate they are not directly
509 driven by basinward-dipping normal faults, but form by salt and overburden translation
510 in response to extension further updip (Figs. 7-8, 10 and 12-13). Their asymmetry and
511 landward-vergence also discredit the hypothesis that they are driven purely by salt
512 expulsion, because in that case they would be symmetric and with vertically-aligned
513 axial-traces (i.e. bowls *sensu* Rowan and Weimer, 1998). Expulsion, nevertheless, plays a
514 second-order control on their kinematics, because as RSBs thicken, they impose
515 increasing load onto the underlying salt and, as the salt thins, they tend to translate
516 progressively slower (Jackson and Hudec, 2005; Pichel et al., 2018a). This increases the
517 relative importance of load-driven subsidence and salt expulsion over time until the salt
518 is drastically thinned, resulting in progressively more symmetry in the upper section of
519 the RSB (Figs. 7-8 and 12-13).

520 A total of 9-10 km basinward translation is estimated by measuring the distance of the
521 first, basinwardmost onlap point and/or depositional axial-trace to the top of the base-
522 salt ramp (Figs 7-8) (c.f. Jackson and Hudec, 2005). This amount of translation, however,
523 only accounts for the period when the salt canopy was already formed because
524 individual sheets would not have merged after being deeply buried by sediments. They
525 are likely to have coalesced early, immediately after their extrusion over a depositional
526 hiatus prior to, or early in, the history of the RSBs, indicating that additional, early salt
527 translation occurred without having a record in the overburden that allows its
528 quantification. The contractional and extensional domains associated with these RSBs
529 (Figs. 10 and 12) are, therefore, formed after or late during the coalescence of individual

530 salt sheets, indicating their development is controlled by the relief at the base of the
531 canopy (c.f. Dooley et al., 2018).



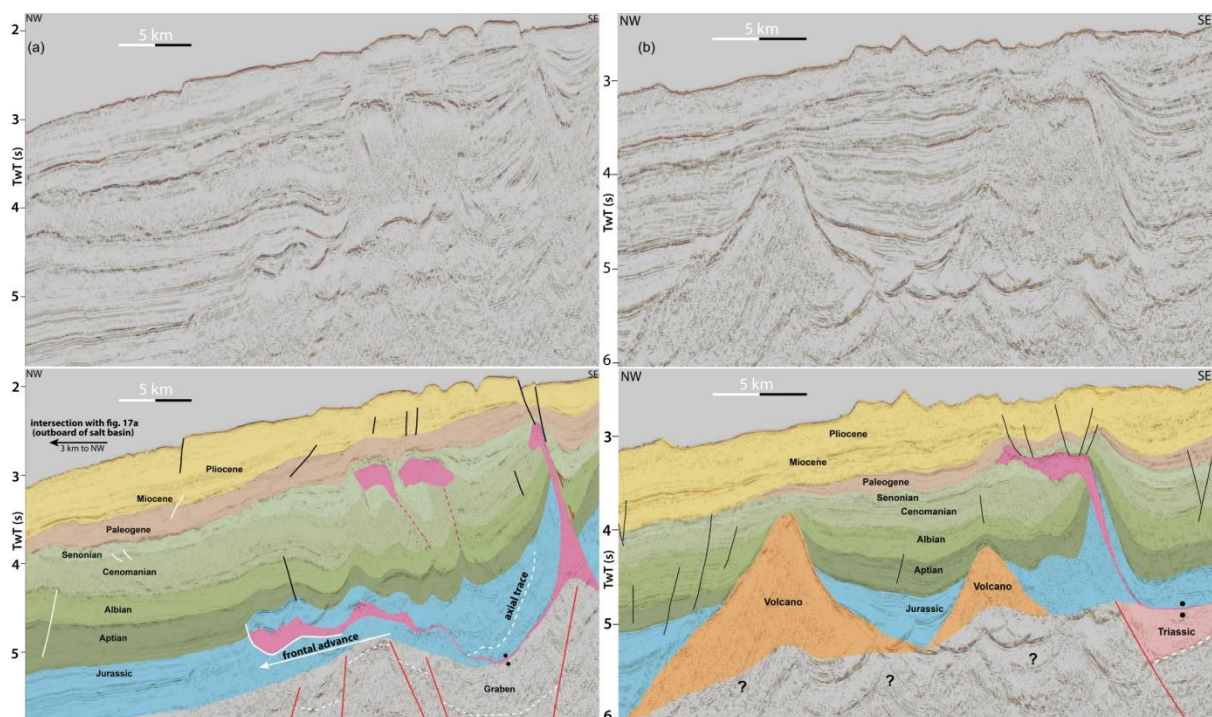
532
533 *Figure 12: Uninterpreted and interpreted 3D seismic section showing complex kinematics on top of*
534 *allochthonous salt canopy in the Essaouira Basin, with pairs of updip extension, translation defined*
535 *by ramp-syncline basins (RSB) and downdip uplift and contraction. Mesozoic sub-salt strata also*
536 *show similar alternation and multiphase evolution of minibasins and salt feeders that originate*
537 *the allochthonous salt sheets, with zones of basinward-thickening passing downdip to zones of*
538 *uplift and basinward-thinning. Pre-salt rift structures (red dashed lines) are estimated based on*
539 *supra-salt architectures and wedge geometries and truncation patterns below autochthonous salt.*



541 *Figure 13: (a) Uninterpreted and (b) interpreted 3D seismic section zooming on ramp-syncline*
 542 *basins (RSB) systems formed above the largest allochthonous salt canopy offshore Morocco. (c)*
 543 *Schematic diagram illustrating the complex kinematics associated with gliding on top of*
 544 *allochthonous salt sheets with drastic initial thickness variations and very irregular base-salt*
 545 *topography, which results in development of alternate domains of updip extension, translation*
 546 *(RSB) and downdip contraction. Translation and salt expulsion work in tandem generating*
 547 *accommodation, with expulsion becoming gradually stronger where salt was initially thicker (e.g.*
 548 *feeders).*

549 4.2.3. Safi Basin

550 The northernmost segment, termed the Safi Basin, corresponds to a considerably
 551 narrower (40-45 km wide) and steeper (c. 5° of base-salt dip on average) salt basin,
 552 with reduced salt volume and resultant smaller number of structures than segments
 553 further south (Figs. 3 and 14-16). This segment is also characterized by the thinnest
 554 overburden in the study-area, being on average only 3.5-4 km thick (Figs. 14-16).



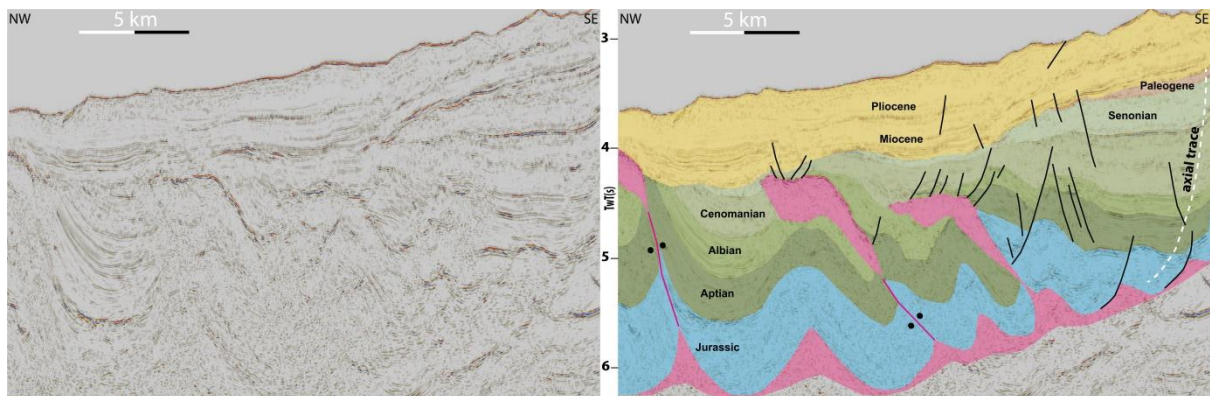
555 *Figure 14: Uninterpreted and interpreted sections of (a) southern portion of Safi segment showing*
 556 *8 km wide salt nappe and salt-cored folds indicating frontal advance from the downdip edge of the*
 557 *salt basin over a c. 10 km wide pre-salt graben. A thick Jurassic-Cretaceous minibasin forms by*
 558 *increased subsidence near the graben basinward-dipping fault; passing downdip to a sub-vertical*
 559 *squeezed feeder with multiphase growth and small salt tongue at its crest. In (b) large volcanoes*
 560 *defined the downdip edge along the centre of the Safi segment, acting as strong buffers to downdip*
 561 *salt flow (Tari and Jabour, 2013), favouring contraction and upward movement of salt resulting in*
 562

563 *development of a steep seaward-leaning feeder by reverse shearing and allochthonous sheet.*
564 *Vertical Exageration is c. 5-fold based on an average velocity of 4000m/s.*

565 To the southwest, near the Essaouira segment, a c. 10 km wide salt nappe has advanced
566 c. 10 km basinward from the downdip edge of the salt basin defined by a relatively
567 symmetric 10 km wide pre-salt graben (Fig. 14a). This salt nappe comprises a frontal
568 thrust and salt-cored fold belt linked updip to a c. 3.5 km thick, welded Jurassic-Upper
569 Cretaceous minibasin. The minibasin contains an asymmetric, landward-thickening
570 Jurassic growth section defined by a basinward-dipping axial-trace characteristic of
571 ramp-syncline basins (RSBs, Pichel et al, 2018a). This suggests the minibasin formed by
572 a combination of load-driven subsidence and translation over thick salt at the updip
573 edge of the graben, promoting basinward salt expulsion towards the nappe (Fig. 14a).
574 Over its updip footwall, a basinward-verging nearly-welded salt wall with a c. 1 km wide
575 tongue at its crest is associated with Jurassic-Early Albian growth strata showing
576 evidence of subsidence towards the wall; whereas Late Albian-Paleogene strata are
577 upturned and uplifted, suggesting later inversion (Fig. 14a). Cenozoic salt movement is
578 less pronounced in this segment, as salt structures become buried by a Late Cretaceous-
579 Paleogene section, possibly due to the smaller salt supply in the area (Fig. 14).
580 Nevertheless, ongoing activity is recorded by a few structures, as seen by normal
581 faulting at the crest of the basinward-leaning and rising diapir at the updip edge of the
582 graben (Fig. 14a).

583 Large (3-4 km high and at least 10 km wide) flat-based conical features interpreted as
584 volcanoes (Dunlap et al., 2010; Tari and Jabour, 2013) occur in the central portion of
585 this segment (Fig. 14b). The base of the volcanoes occur at the same stratigraphic level
586 as the base of autochthonous salt suggesting both originated at/near the same time at
587 the end of rifting during the Late Triassic-Early Jurassic (Fig. 14b). These tall volcanoes

588 generated additional topography during salt deposition with salt being deposited
 589 around but not on top of them. They acted as topographic barriers, limiting early
 590 (Jurassic-Lower Cretaceous) downdip gliding and salt advance, and thus, inhibiting the
 591 development of a salt nappe in this part of the basin (Figs. 3 and 14b) (Tari and Jabour,
 592 2013). Additionally, they promoted increased and early downdip contraction and
 593 upward salt flow on their landward side (c.f. Ferrer et al., 2017), as shown by uplift and
 594 reverse shearing/thrusting of the updip minibasins against seaward-leaning squeezed
 595 diapirs during the Jurassic-Early Cretaceous (Figs. 14b and 15). This also resulted in
 596 earlier development of small (3-5 km wide) salt sheets during the Albian-Cenomanian
 597 due to diapir squeezing (Fig. 14b and 15).

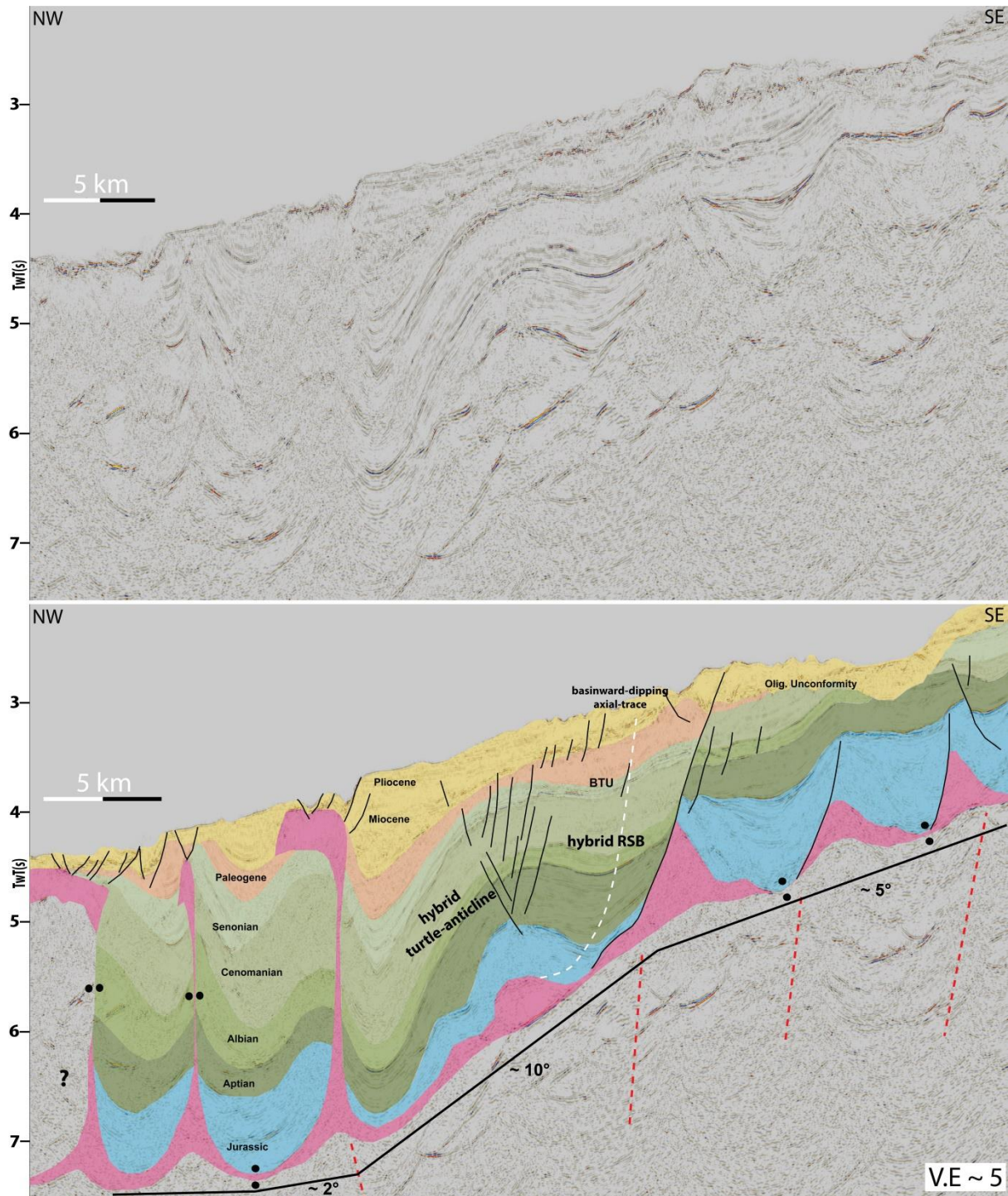


598
 599 *Figure 15: Uninterpreted and interpreted sections of Safi segment showing early (Albian-*
 600 *Cenomanian) development of allochthonous salt tongues associated with counter-regional,*
 601 *seaward-leaning feeders formed by contraction and thrusting of the hangingwall over the feeders.*
 602 *Minor updip extension (small salt rollers and basinward-dipping normal faults) occurs during the*
 603 *Jurassic, passing upwards to an asymmetric, landward-dipping growth section, possibly associated*
 604 *with a ramp-syncline basin.*

605 Further northwards, near the limit of this segment, the margin becomes steeper and a
 606 large (30-35 km) linked gravity-driven system is developed (Fig. 16). This system is
 607 characterized by updip Jurassic-Aptian rafts and associated 2-4 km amplitude salt
 608 rollers and basinward-dipping listric faults. This domain transitions downdip to a 5-10
 609 km wide translational province formed over a considerably steeper (c. 10°) salt
 610 detachment associated with a large base-salt ramp (Fig. 16).

611 In this translational domain, a hybrid turtle anticline formed by a combination of salt
612 expulsion and updip extension over a large (3.5 km tall), basinward-dipping normal
613 fault with a ramp-flat geometry (*sensu* McClay, 1990, 1996). This fault is defined
614 basinward by a Jurassic extensional-rollover, passing upwards to an extension-driven
615 and salt-influenced RSB (c.f. McClay, 1990, 1996; Roma et al., 2018a); recording c. 7 km
616 of salt and overburden downdip translation (Fig. 16). The hybrid turtle anticline
617 overlies an inflated salt (c. 1 km thick anticline) at its centre (Fig. 16), having a different
618 geometry to classical turtle anticlines (*sensu* Vendeville and Jackson, 1992b) in which
619 the underlying salt is nearly or completely exhausted (c.f. Jackson and Hudec, 2017).
620 This implies that subsidence and salt expulsion are not focused at the centre of the
621 minibasin and that these hybrid examples are primarily driven by extension and
622 translation. Subsidence is focused over the normal fault, so while sediments accumulate
623 there, previous strata translate and rotate basinward resulting in a landward-thickening
624 succession (hybrid RSB) and downdip salt inflation (Fig. 16). At the downdip end of this
625 turtle, a thinned Jurassic-Aptian section overlying nearly welded salt passes upward to
626 thickened Cenomanian-Paleogene strata, both of which synformally folded and
627 associated with a vertical squeezed feeder (Fig. 16).

628 In the downdip domain, highly squeezed sub-vertical salt walls associated with buckle-
629 fold geometries within their minibasins and 2-5 km wide allochthonous salt sheets
630 indicate deformation was mainly driven by contraction (Fig. 16). As evidenced by
631 extension and translation further updip, contraction occurred as the system moved over
632 a base-salt contractional hinge at the downdip end of the basin where the base-salt
633 flattens and flow decelerates abruptly (Fig. 16) (c.f. Dooley et al., 2016; 2018).

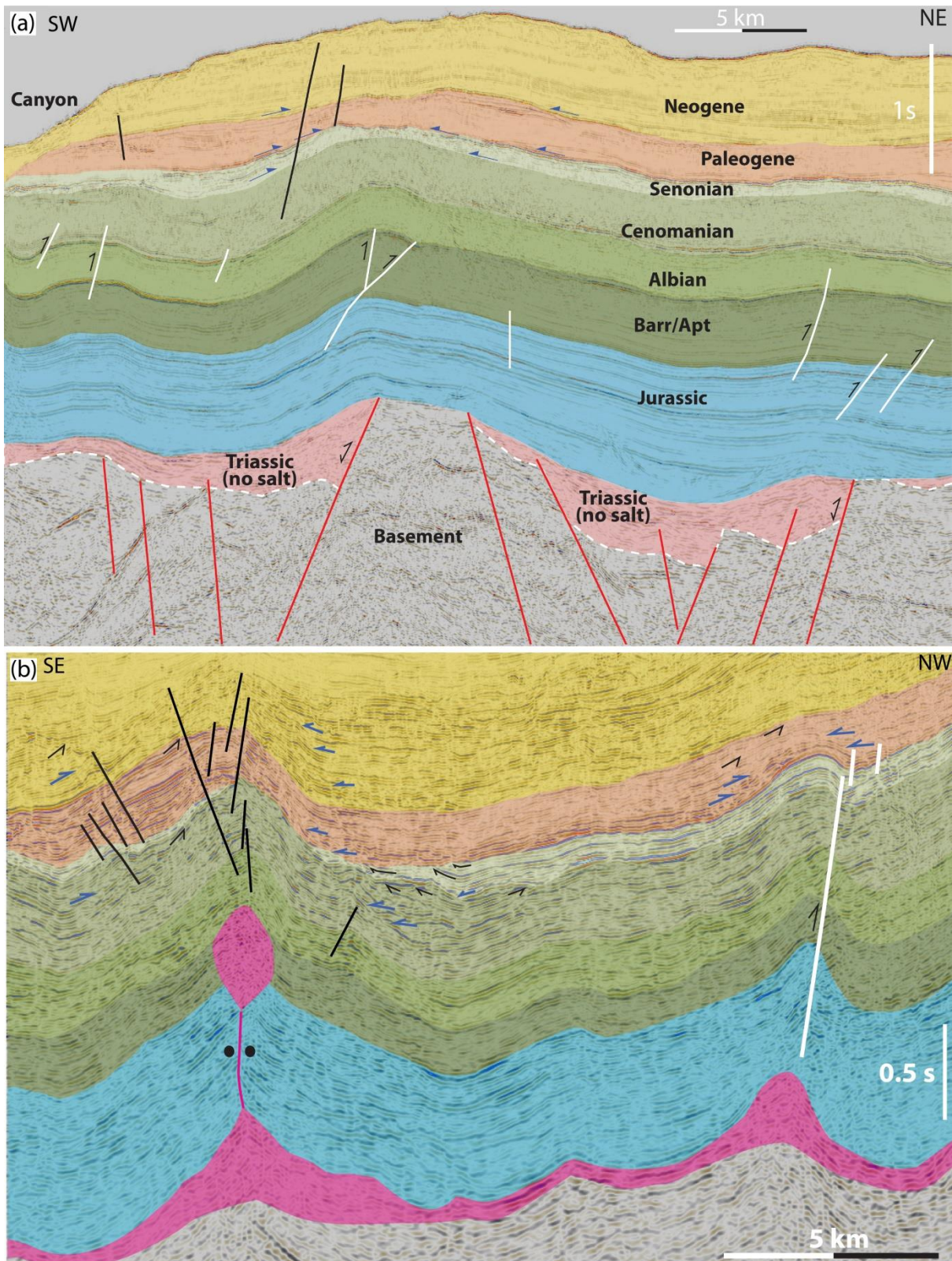


634
 635 *Figure 16: Uninterpreted and interpreted sections of the northern end of Safi Basin (Tari and*
 636 *Jabour, 2013) showing a narrow kinematically-linked system of updip extension with basinward-*
 637 *dipping normal faults and roller; intermediate translation with a hybrid RSB and turtle anticline*
 638 *over a steep basinward-dipping base-salt ramp; passing downdip to highly-squeezed sub-vertical*
 639 *diapirs and salt tongues. Vertical Exageration is c. 5-fold based on an average velocity of 4000m/s.*

640 **5. Impact of thick-skinned tectonics**

641 The effects of thick-skinned contraction related to the Alpine/Atlas Orogeny have been
642 described by a number of authors, both onshore and offshore along the margin (Hafid et
643 al., 2000; 2006; Tari et al., 2012; 2017, Tari and Jabour, 2013; Vergés et al., 2017).
644 Although recognized to have an impact on salt tectonics and basin morphology, these
645 previous studies did not investigate how these broadly N-S-oriented contractional
646 events affected the kinematics and style of salt deformation offshore.

647 A series of NW-SE-trending basement-involved folds had been recognized outboard of
648 the salt basin along the Safi segment by Tari et al. (2012), formed by reactivation and
649 inversion of syn-rift normal faults (Fig. 17a) (Tari and Jabour, 2013). As these folds are
650 located basinward of the salt basin, thickness variations and growth strata can be used
651 as confident indicators of the timing and kinematics of these salt-unrelated events. A
652 broadly isopachous Jurassic-Cenomanian succession is folded over 10-15 km
653 wavelength basement-involved folds, cored by inverted syn-rift faults and uplifted
654 basement (Fig. 17a). The folds present rounded to box-fold geometries, being offset by
655 predominantly NE-verging reverse faults (Fig. 17a). Senonian-Paleogene growth strata
656 onlap and thin towards the crest of this structure, being capped by a broadly isopachous
657 folded Neogene succession with greater thickness variations occurring in the Paleogene
658 interval (Fig. 17a). These stratal patterns indicate that thick-skinned contraction started
659 during the Senonian, became stronger during Paleogene-Miocene and reduced during
660 the Pliocene-recent, although it is still ongoing as demonstrated by the folded present-
661 day seafloor (Fig. 17a).



662
 663 Figure 17: (a) Strike-oriented section outboard of the salt basin in Safi, showing inversion of pre-
 664 salt normal faults, basement-involved folding and reverse faulting of a broadly isopachous
 665 Jurassic-Cenomanian succession overlapped by Senonian-Neogene strata. (b) Strike-oriented section
 666 at the shelf-edge in Agadir Basin showing two pulses of broadly N-S contraction in the Late
 667 Cretaceous and Miocene-Pliocene. Normal faults in black and reverse faults in white lines.

668 *Erosional truncation indicated black arrows and onlaps by blue arrow denoting the main period of*
669 *tectonic activity.*

670 Further south, near the large salt nappe in Essaouira, there is evidence of both salt-
671 related and thick-skinned N-S contraction (Fig. 4). North of the salt nappe, the thick,
672 broadly tabular Jurassic-Cenomanian interval is folded and onlapped by Senonian-
673 Paleogene growth strata and truncated by the BTU and Paleogene unconformities (Fig.
674 4). Over the southern edge of the nappe, a triangular salt roller is associated with a
675 northward-dipping listric normal fault with Jurassic asymmetric growth strata at its
676 hangingwall (Fig. 4). Lower Cretaceous growth is dramatically reduced, as seen by a
677 nearly isopachous, albeit folded, section that is uplifted above regional over the fault
678 and onlapped by Senonian-Paleogene strata, indicating that the fault and earlier
679 extensional rollover were inverted during this time (Fig. 4).

680 At the updip end of the basin between Agadir and Essaouira (Fig. 3), a NW-SE-oriented
681 profile images another example of roughly W-E salt-related contractional structures
682 (Fig. 17b). A N-NW verging salt-cored box-fold and a tear-drop diapir developed in the
683 shelf involving a broadly isopachous Late-Jurassic-Early-Cretaceous interval that is
684 onlapped by late Cenomanian-Paleogene growth strata and truncated by equivalent
685 unconformities (Fig. 17b). Earlier, Middle-Jurassic growth occurred but this was minor
686 as indicated by a broadly tabular Aptian-Cenomanian interval that was later upturned
687 and broken apart by the squeezed diapir (Fig. 17a). Although there is no clear evidence
688 of basement-involved reactivation due to sub-salt resolution issues (Fig. 17b), the E-W
689 orientation of these highly squeezed salt structures, location at the shelf, and timing of
690 movement indicate they are also associated with the same Late Cretaceous-Cenozoic
691 contractional event (Fig. 17). Due to their position and orientation, we may also

692 speculate that they correspond to the continuation of a salt-cored fold at the edge of the
693 continent (Cap-Ghir Anticline, Lubber, 2017)

694 These lines of evidence can be extended towards the more complex, central areas of the
695 basin, where pronounced salt tectonics partially obscures signals of basement-involved
696 contraction. The widespread occurrence of shortening-driven minibasins and squeezed
697 diapirs, many of which currently active and uplifting thick roofs (up to c. 1.5 km) over
698 the shelf and entire slope in Agadir-Essaouira (Fig. 5), suggest an important
699 contribution from late thick-skinned contraction. 3D seismic data, which offer better
700 illumination of sub-salt intervals, shows proximal areas where the autochthonous salt
701 and entire overburden are uplifted c. 1-2 km above regional at the north-northeast of
702 Essaouira (Figs. 10-11).

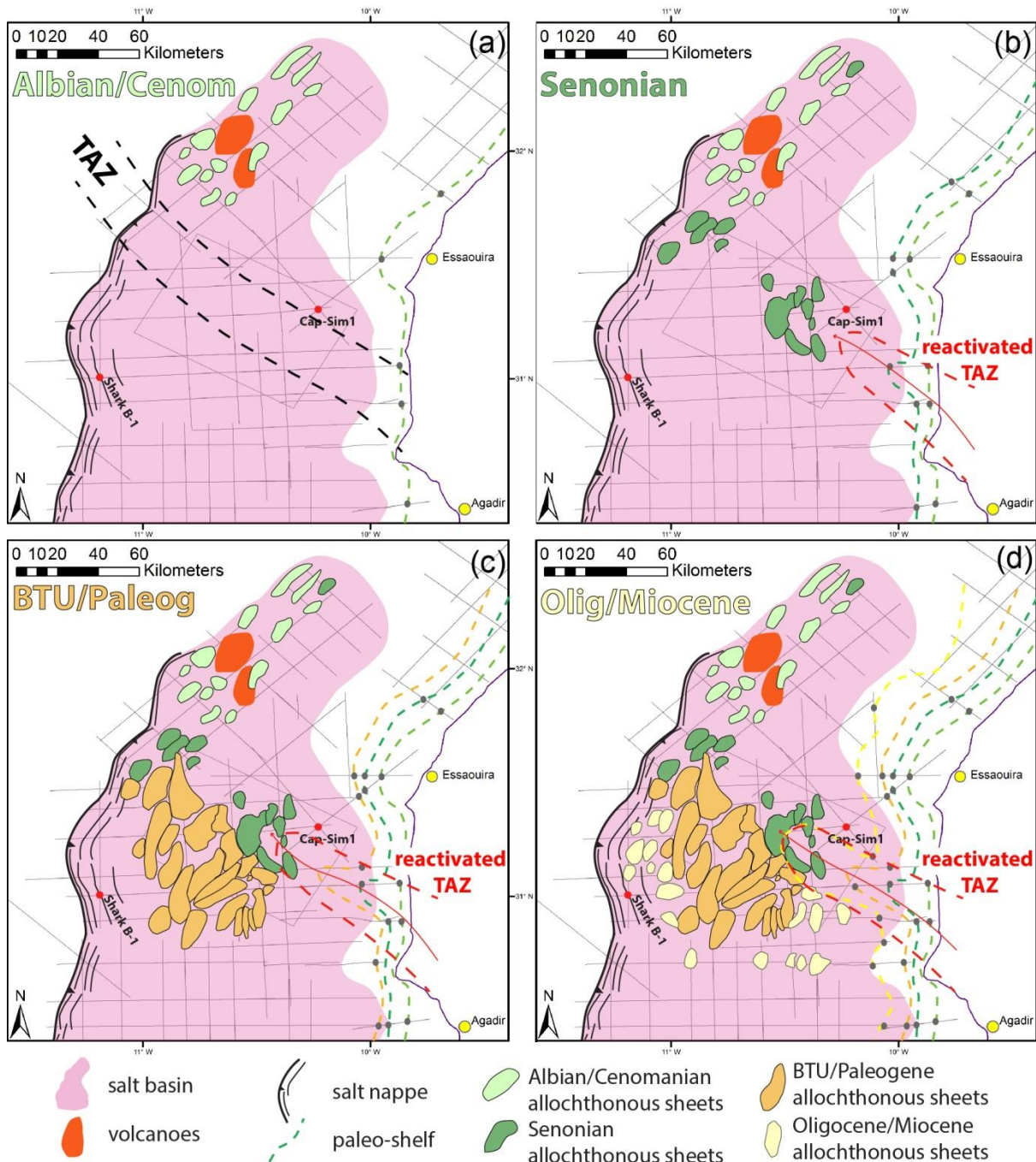
703 Although the data does not afford clear visualization of basement structures
704 throughout, where the allochthonous salt is thinner, it is possible to observe pre-salt
705 geometries (i.e. tightening and uplift of syn-rift hangingwall folds, figs. 10-11) that
706 indicate contraction and inversion of syn-rift structures. This area coincides with the
707 location of the Tafelney Accommodation Zone (TAZ, Tari and Molnar, 2005; Tari et al.,
708 2012), an oblique NW-SE syn-rift high that could have acted as a favourably-oriented
709 weakness zone preferentially accommodating most of the N-S to NE-SW contraction in
710 the basin. This resulted in additional contraction of salt feeders and diapirs, and further
711 tilting that enhanced basinward gliding at the allochthonous level in this portion of the
712 basin (Figs. 7-8 and 10-13). Moreover, it could have favoured an outward, NW-oriented
713 salt flow, sub-parallel to the NW-plunging axis of the uplifted Tafelney Accommodation
714 zone, and may explain the NE-SW orientation of salt sheets oblique to the margin (Figs.
715 1, 3 and 18).

716 **6. Timing and mechanisms of allochthonous salt sheets generation**

717 Multiple allochthonous salt sheets with variable geometries, dimensions, orientation
718 and evolution occur over the Essaouira-Safi segments (Figs. 7-13 and 18). Features
719 observed include sub-vertical to seaward-leaning diapirs with small (2-5 km wide) salt
720 tongues, as well as large allochthonous salt sheets and canopies up to 35 km wide, 45
721 km long and 2.9 km thick (Figs. 7-8 and 18). Extrusion and/or emplacement of
722 allochthonous salt occurred during variable periods along the margin, with four major
723 phases recognised from Albian-Cenomanian to Oligoce-Miocene (Fig. 18a-d) generally
724 related to major erosional unconformities and/or depositional hiatuses (Figs. 7-13).

725 **6.1. Albian-Cenomanian**

726 The first allochthonous sheets formed during the Late Albian-Cenomanian in the
727 northernmost Safi segment. These are characterized by NE-oriented, 3-5 km wide salt
728 tongues that can reach up to 10 km of length (Fig. 18a). These bodies are usually
729 associated with steeply-dipping landward growth strata uplifted and thrust over
730 footwall growth strata (Figs. 14b-15). These geometries indicate they formed by
731 contraction at the downdip end of the basin and over base-salt contractional hinges
732 (*sensu* Dooley et al., 2016) or against the large volcanic/basement buttresses.



733
 734 *Figure 18: Maps showing the sequential evolution of allochthonous salt sheets along the Moroccan*
 735 *margin during four main phases: (a) Albian-Cenomanian, (b) Senonian, (c) BTU-Paleogene, and*
 736 *(d) Oligo-Miocene.*

737 **6.2. Senonian**

738 The second generation of allochthonous salt occurred during the Senonian, with the
 739 development of c. 5 km wide allochthonous sheets in the south of Safi and northeast of
 740 the Essaouira (Figs. 7-8), with only one small salt tongue developing further north at the
 741 edge of the Safi Basin (Fig. 15 and 18b). The first allochthons appear at the landward

742 portion of Essaouira, in an area defined by the culmination of the basement-involved
743 and salt-influenced NW-SE high that probably formed by reactivation of the syn-rift TAZ
744 (Fig. 10-11 and 18) and is regarded as the offshore continuation of the Atlas Fold-Belt
745 (Hafid et al., 2000; 2006; Tari et al., 2017). These Senonian sheets have more complex
746 geometries than the earlier, Albian-Cenomanian ones, being drastically thinned and
747 associated with sets of updip basinward-dipping normal faults (roho) that indicate
748 greater downdip salt evacuation and gliding (Figs. 10-11).

749 **6.3. BTU-Paleogene**

750 The third generation of allochthonous salt is associated with the regional expression of
751 the major erosional BTU unconformity (Tari and Jabour, 2013) and coincides with the
752 peak of thick-skinned contraction along the margin (Fig. 18c). Contraction continued to
753 propagate offshore and by this time was affecting the entire salt basin (Fig. 17). This
754 resulted in the largest volume of salt being extruded over/near this regional
755 unconformity and development of the largest and thickest canopy systems, which
756 formed by coalescence of smaller sheets from Senonian to Paleogene times (Fig. 9).
757 These sheets acted as bathymetric highs that, under low sediment input conditions
758 typical of uplifted areas, were not deeply buried and, therefore, were able to advance
759 over thin syn-kinematic sediments and to merge with other sheets basinward (Fig. 18).
760 Most of the allochthonous salt in Safi was already emplaced and their feeders exhausted
761 by the end of Cretaceous due to contraction at the downdip end of the basin, so no new
762 allochthons developed.

763 **6.4. Oligo-Miocene**

764 The final generation of allochthonous salt occurred over the downdip edge of the salt
765 basin and further south at the transition to the Agadir segment (Fig. 18d), represented

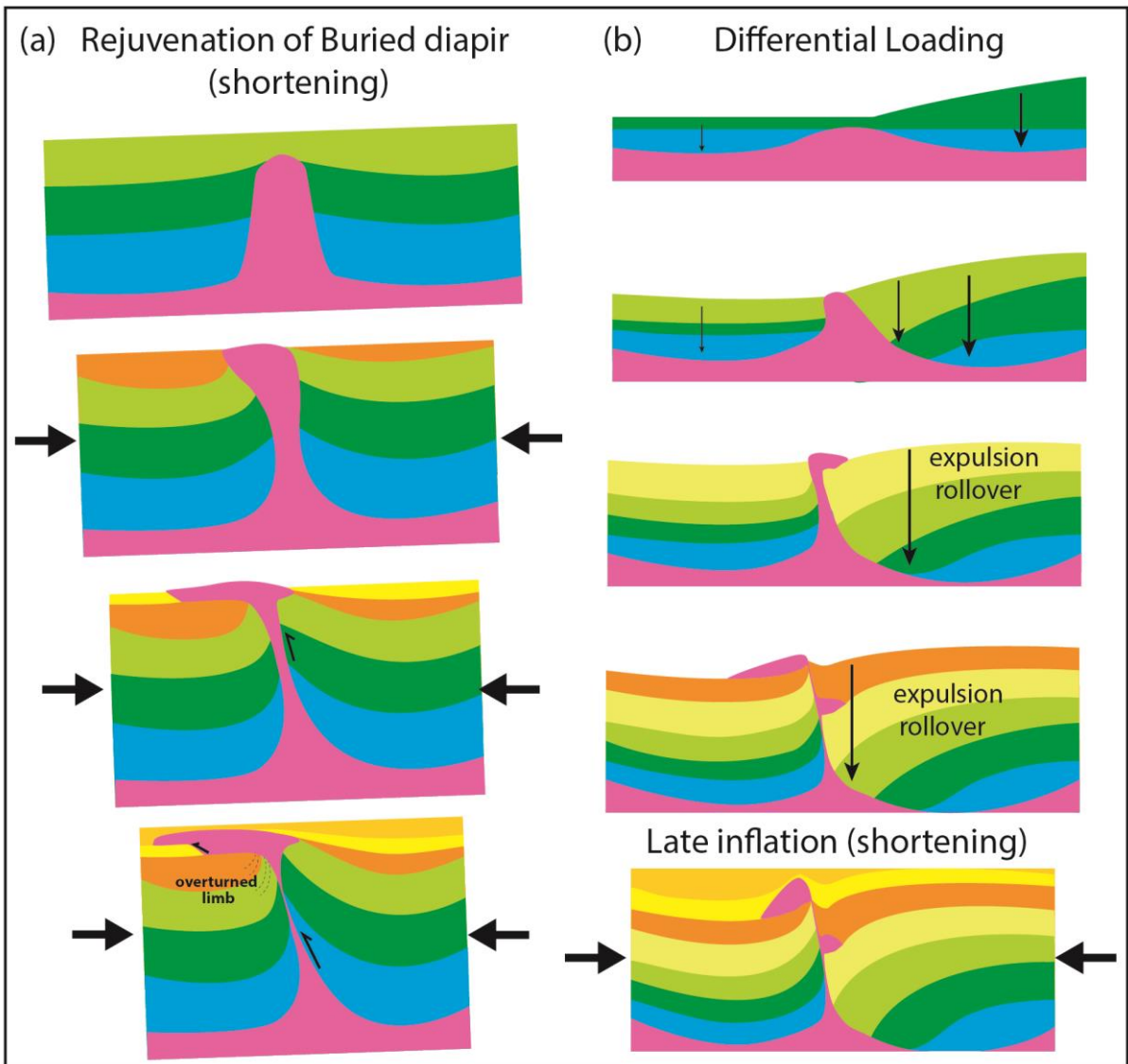
766 by smaller (1-3 km wide) salt tongues at the crest of sub-vertical diapirs (Fig. 7). These
767 features appear to have formed by renewed pulses of contraction during the Oligo-
768 Miocene, being highly inflated (1.5-2.5 km thick) and associated with frontal thrusts and
769 uplift of pre-kinematic roofs, suggesting they formed by thrusting rather than extrusion.

770 **6.5. Mechanisms**

771 The earliest generation of allochthonous salt in the Safi segment is explained by more
772 abrupt gliding caused by the steeper and narrower salt detachment and presence of
773 large downdip pre-salt barriers (e.g. volcanoes) enhancing contraction (Figs. 14-16).
774 The occurrence of Late Cretaceous sheets over the zone of uplifted basement at the
775 updip portion of Essaouira suggests that the offshore continuation of a thick-skinned
776 fold-belt acted as the main control on their generation, favouring diapir squeezing, salt
777 extrusion and enhancing downdip gliding (Figs. 10-11). The next and most expressive
778 generation of allochthonous salt occurred further basinward associated with a major
779 erosive event (i.e. BTU, Tari and Jabour, 2013) and propagation of basement-involved
780 contraction, resulting in larger volumes of salt reaching the surface (Fig. 7-9).
781 Generation of allochthonous salt continued to propagate basin- and southward of the
782 thick-skinned fold-belt with thrusting of salt tongues in the Oligo-Miocene (Fig. 7).

783 Salt sheets formed mainly by salt extrusion near or on the paleo sea-floor, commonly
784 associated with major hiatuses and/or regional erosional events (e.g. Hudec and
785 Jackson; 2006) (Fig. 7 and 10-13). Later Oligo-Miocene salt tongues seem to have
786 involved thrust-piercement (c.f. Hudec and Jackson 2007), as they are usually narrower,
787 highly-inflated and offset a thin (200-300 m) pre-kinematic roof (Fig. 7-8). The main
788 mechanism of emplacement of allochthonous sheets is, therefore, contraction of sub-
789 vertical feeders (Fig. 19a) related to both gravity and thick-skinned tectonics. In both

790 cases, hangingwall strata are generally thinner and uplifted relative to the downdip
 791 footwall (Figs. 11-13, 15 and 19a), occasionally showing fold geometries suggesting
 792 reverse shearing/faulting (Figs 7-8, 11 and 15) (Shaw et al., 2005).



793
 794 *Figure 19: Simplified, area-balanced kinematic models of end-member mechanisms leading to*
 795 *development of allochthonous salt sheets in the Essaouira-Safi Basins: (a) rejuvenation of buried*
 796 *sub-vertical diapirs and (b) basinward expulsion rollover.*

797 The second mechanism is associated with landward-dipping feeders in which the updip
 798 minibasin subsides relative to the downdip one, being commonly associated with
 799 basinward-thickening expulsion rollovers (Figs. 7, 13a and 19b). In this mechanism, an
 800 earlier salt ridge forms a sea-floor topographic barrier that results in ponding of deep-

801 water sediments (Fig. 19b). This produces loading that gradually expels salt seawards,
802 generating seaward-leaning diapirs and basinward-thickening folded strata defining an
803 expulsion rollover (c.f. Ge et al., 1997; Krézsek et al., 2007) (Fig. 18b). This style of
804 growth predominates in the Essaouira segment and, interestingly, occurs in its mid-
805 slope portion, alternating with contraction-driven structures on both sides (Fig. 7).

806 **7. Discussion**

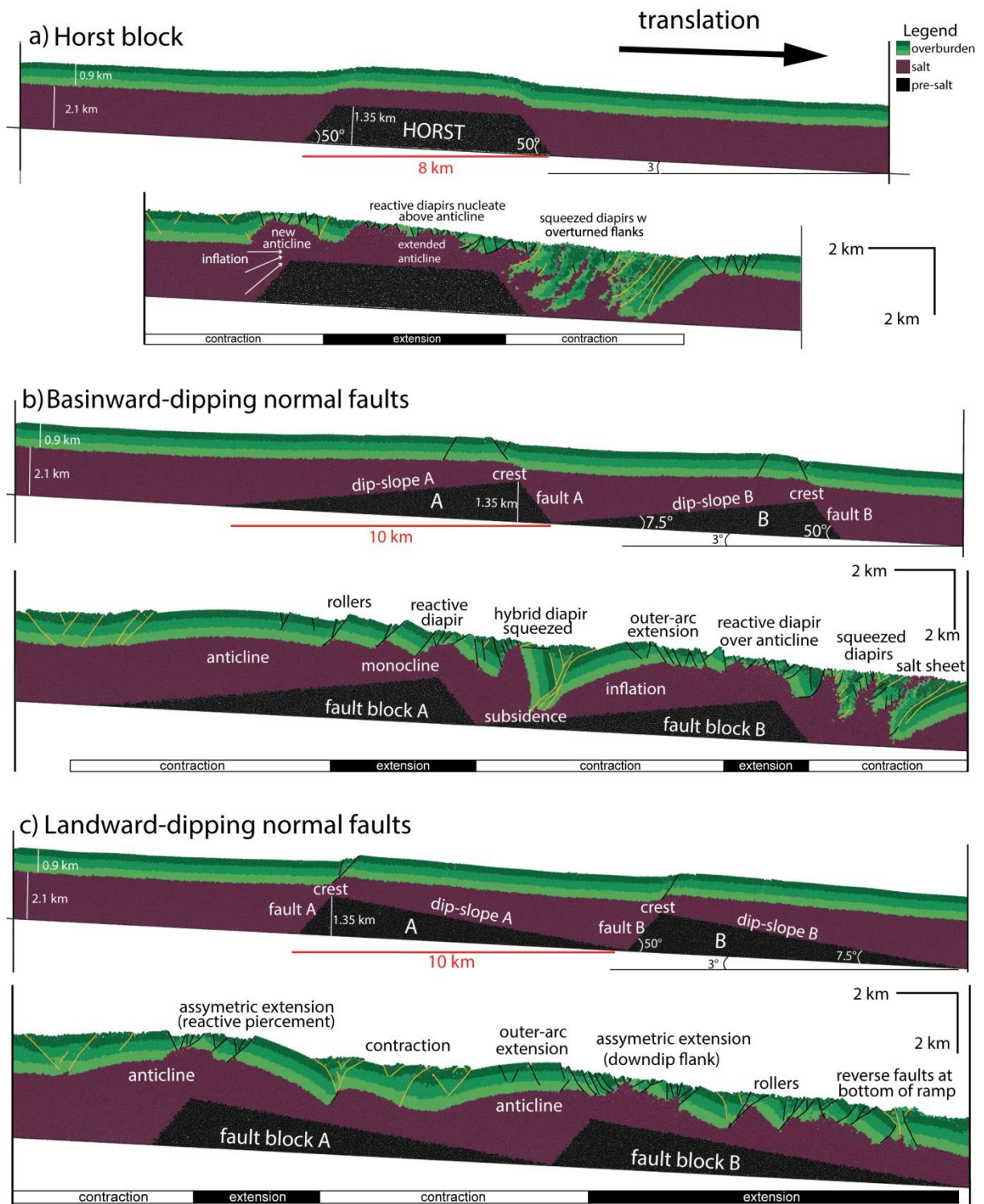
807 **7.1. Influence of base-salt relief on allochthonous salt flow**

808 Recent physical (Dooley et al., 2016; Dooley and Hudec 2016; Ferrer et al., 2017) and
809 numerical (Pichel et al., 2018a,b) modelling has shown how pre-salt structures and
810 base-salt relief act as important controls on salt tectonics by promoting flux variations
811 that result in more intricate distribution of structural styles (Fig. 20). Salt and
812 overburden translation over pre-salt horsts results in initial inflation and contraction at
813 their updip edges (landward-dipping base-salt ramps); and later extensional collapse as
814 the salt gradually thickens and accelerates over the horst (base-salt flats, fig. 20a).
815 Conversely, translation over their downdip edges (basinward-dipping base-salt ramps)
816 produces a zone of salt subsidence limited updip by extension at the top and contraction
817 at the bottom of the ramp (Fig. 20a) (Dooley et al., 2016; 2018; Pichel et al., 2018a, b).

818 In the case of tilted blocks, salt flux variations, multiphase diapirism and alternation of
819 structural styles are even more pronounced, resulting in pairs of extensional-
820 contractional zones (Fig. 20b-c). These zones have varying widths and deformation
821 magnitudes according to their development over steep or gentle base-salt ramps
822 defined by pre-salt faults and footwalls respectively (Pichel et al., 2018b). Although
823 these models do not include syn-kinematic sedimentation, landward-thickening
824 minibasins (i.e. ramp-syncline basins, Jackson and Hudec, 2005) are expected to

825 develop in these settings above or downdip of base-salt ramps given that aggradation
826 rates are lower than translation rates (RSBs, c.f. Pichel et al., 2018a; Dooley et al., 2018).

827 A series of RSBs and pairs of extension-contraction zones were identified over
828 allochthonous sheets in a level with higher seismic resolution (Figs. 7-8 and 10-13),
829 demonstrating evidence of salt and overburden translation (i.e. gliding) over complex
830 base-salt relief. Gliding generated basinward-dipping listric normal faults and
831 extensional rollovers at the rear of salt sheets and near the top of basinward-dipping
832 ramps at their base (Figs. 7-8 and 12-13). Immediately downdip, intermediate zones of
833 translation were commonly characterized by landward-dipping gently-folded and
834 sigmoidal growth strata (RSBs) directly onlapping the top allochthonous salt without
835 any direct evidence of faulting (Figs. 7-8 and 12-13). These RSBs were defined by
836 basinward-dipping axial traces and finished updip immediately above the top of base-
837 salt ramps (Figs. 7-8, 10 and 12-13). Downdip of the RSBs, gliding was accommodated
838 by salt inflation, overburden contraction and uplift, and occasionally, early-stage open-
839 toe advance when the salt sheet frontal edge advanced without roof sediments to record
840 contraction (Figs. 5 and 8). Similar patterns of allochthonous salt flow and complex
841 distribution of supra-salt structural styles have been recently modelled by Dooley et al.
842 (2018) and explained by the interplay between dynamic salt budget and variations of
843 base-salt relief associated with coalescence of sheets.



844
 845 *Figure 20: Discrete-Element models simulating early-stage gliding over pre-salt structures and*
 846 *equivalent base-salt ramps: (a) horst block, (b) tilted fault-blocks defined by basinward-dipping*
 847 *normal faults and in (c) tilted blocks defined by landward-dipping faults (adapted from Pichel et*
 848 *al., 2018b).*

849 Although recently recognized in the Gulf of Mexico (Peel, 2018; pers. comm), and briefly
850 described in Pichel et al. (2018a), allochthonous salt-detached RSBs have never been
851 analysed in detail. As shown by novel numerical models (Pichel et al., 2018a),
852 translation results in salt subsidence and syn-kinematic deposition above the base-salt
853 ramp; and as the system evolves, strata move out of the locus of subsidence being
854 rotated and uplifted while new sediments are deposited over the ramp (Figs. 10-13).
855 Where RSBs form, they impose additional loading onto the salt and are, therefore,
856 commonly associated with coeval expulsion below them and inflation downdip.

857 At the allochthonous salt level, these RSBs typically develop over and/or near sub-
858 vertical squeezed feeders, being highly rotated, asymmetric and with abrupt onlaps
859 towards the top salt (Figs. 8, 10 and 12-13). This indicates relatively fast flow and
860 subsidence rates that can be attributed to an initially higher salt budget above feeders
861 (c.f. Dooley et al., 2018). Once the feeders are exhausted due to shortening and/or
862 loading, the salt supply is reduced and continuous subsidence and loading within the
863 RSBs tend to expel the underlying salt seaward, thinning the salt above the feeders
864 (Figs. 8, 9c and 12-13). In places, growth strata onlap a drastically thinned/welded
865 landward-dipping segment of the allochthonous sheet indicating more extreme and fast
866 translation over the feeders (Figs. 12-13). The distance of the oldest, basinwardmost
867 onlap within the RSBs to the top of their respective base-salt ramp indicates 5-10 km of
868 downdip gliding at the allochthonous level during the Paleogene-Miocene, at an
869 approximate rate of 0.2 mm/year (0.2 km/Ma). Translation of salt and overburden may
870 have still occurred without development of RSBs in areas without base-salt ramps or
871 when the rates of translation relative to sedimentation were low or the sedimentation
872 controlled by a prograding sedimentary wedge (Pichel et al., 2018a).

873 **7.2. Influence of pre-salt rift structures on regional salt tectonics**

874 The relationships described above for allochthonous salt can be used as a proxy to
875 understand the complex sub-salt structural variation and multiphase growth associated
876 with counter-regional feeders observed in the seismic data (Figs. 7-8 and 10-13). As the
877 salt was deposited during the late syn-rift stage (Tari et al., 2003; 2012), original salt
878 thicknesses are expected to vary dramatically across and within half-grabens (Rowan
879 2014; Jackson and Hudec, 2017). As a consequence, early flow must have been largely
880 influenced by pre-salt rift structures and associated flux variations as shown by
881 numerical (Figs. 20-21) and physical models (Dooley et al., 2016; 2018).

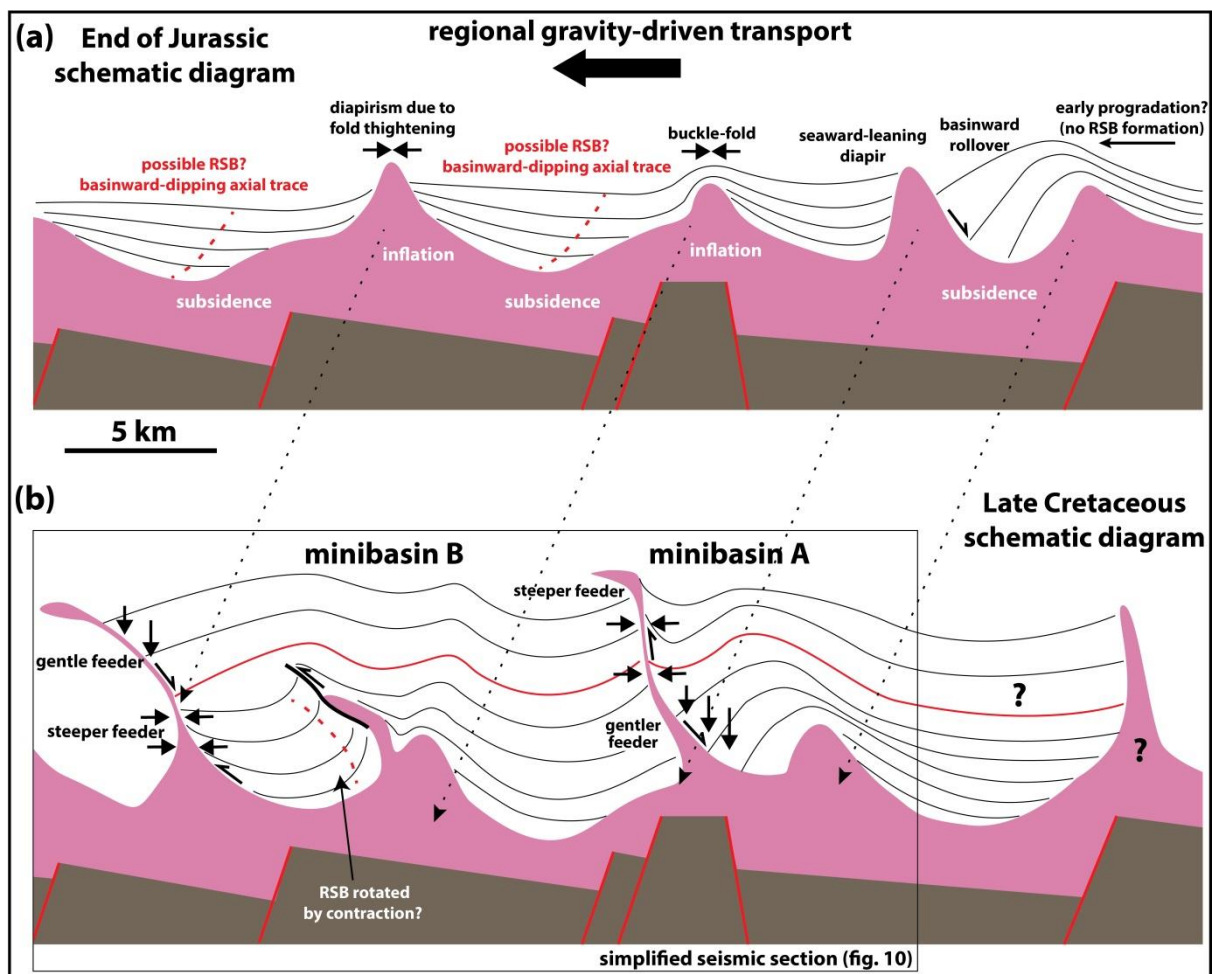
882 The effects of syn-rift salt deposition and thickness variations on detachment
883 connectivity and translation offshore Morocco were first described by Tari et al. (2003)
884 who recognized that translation and salt detachment connectivity were higher in areas
885 of initially thicker salt. Along Essaouira, gliding occurred during the Jurassic-Lower
886 Cretaceous, and possibly Cenomanian, producing the larger salt nappe (c. 15-20 km,
887 figs. 7-8) and greater magnitude of frontal advance than elsewhere along the margin.
888 The largest volume of allochthonous salt and salt structures occurs in this central
889 segment, which is also the widest (Figs. 3 and 7-8). The evidence suggests that the salt
890 was originally thicker and better connected across multiple grabens in the central
891 portion of the basin, where subsidence is expected to be higher. The greater salt
892 thickness and magnitude of downdip translation in this segment resulted in the highest
893 complexity and variable distribution of structural styles along the margin (Figs. 7-13
894 and 21). The presence of a kinematically-linked system of updip extension, translation
895 and downdip contraction in Safi indicates that gliding was also significant across this
896 segment, but occurred over a narrower (c. 40 km) and simpler salt basin affected by

897 fewer pre-salt rift structures (Fig. 15). Despite the small present-day volume of salt
898 structures implying originally thinner salt and limited connectivity relative to Essaouira,
899 gliding in Safi was aided by the greater steepness of the salt detachment (Fig. 14-16).

900 In Essaouira, areas of extension and salt expulsion alternate with areas characterized
901 by overburden uplift and reverse shearing (Figs. 7-8, 10 and 21). Minibasins and their
902 associated feeders show evidence of multiphase growth with early basinward-
903 thickening and subsidence followed by later stratal thinning, upturning and uplift
904 recording an inversion (minibasin A, figs. 10 and 21). Adjacent minibasins exhibit the
905 opposite history, with earlier stratal thinning, reverse shearing and contraction
906 followed by later basinward-thickening and subsidence (minibasin B, figs. 10-21). These
907 multiphase evolution patterns are comparable to models simulating downdip gliding
908 over pre-salt horsts and tilted fault-blocks (Figs. 20-21), showing that despite the
909 typically limited imaging of the pre-salt interval, the recognition of these complex salt-
910 related styles can aid identification of pre-salt structures (Figs. 10-13).

911 According to the models, salt subsidence and cover extension occur above basinward-
912 dipping normal faults where salt is initially thicker (Fig. 20b). Contraction and uplift
913 occur as salt flow is buttressed and salt inflates over landward-dipping faults and/or
914 over the dip-slopes of basinward-dipping faults (Fig. 20b-c). We can, then, infer that the
915 updip minibasin (A, fig. 21) and associated Jurassic rollover originated above a pre-salt
916 low defined by a basinward-dipping normal fault and, as it translated downdip over a
917 pre-salt high, was inverted and uplifted during the Cretaceous. The Jurassic
918 contractional structures of minibasin B formed over this pre-salt high due to early salt
919 inflation and folding (Fig. 21a), being further contracted as they moved downdip over
920 the dip-slope of a tilted fault-block defined by a basinward-dipping normal fault (Fig.

921 21b). Further downdip, Cretaceous strata of minibasin B subsided and thickened
 922 basinward above an area of thick salt over this basinward-dipping normal fault (Fig.
 923 21b). This multiphase evolution is also recorded by the present-day geometry of
 924 squeezed feeders, which dip gently due to increased vertical load when associated with
 925 subsidence and basinward-thickening strata; and steeply due to displacement loading
 926 related to shortening and diapir squeezing (Fig. 21b).



927
 928 *Figure 21: Simplified kinematic model demonstrating the evolution associated with downdip*
 929 *translation of salt and overburden across complex pre-salt rift topography in the Essaouira*
 930 *segment (compare to seismic section on fig. 10). (a) Translation and associated flux mismatches*
 931 *caused by base-salt relief during the Jurassic resulted in subsidence over base-salt lows and salt*
 932 *inflation and contraction over pre-salt highs (horst and crests of tilted fault-blocks). Subsidence*
 933 *favoured the accumulation of prograding sedimentary wedges in more proximal areas and*
 934 *promoted the development of RSBs in more distal areas where the sedimentation rate was lower.*
 935 *(b) Continued translation during the Cretaceous caused early-formed structures to be inverted.*
 936 *Areas of early subsidence were affected by contraction, reverse shearing and uplift over pre-salt*
 937 *highs (minibasin A) and areas of early contraction subsided over pre-salt lows (minibasin B).*

938 *Subsidence resulted in gently-dipping squeezed feeders due to differential sub-vertical loading and*
939 *contraction in steep to sub-vertical feeders due to lateral displacement loading.*

940 The observed alternation of growth patterns associated with sub-vertical feeders and
941 diapirs in Essaouira (Figs. 7-8 and 10) and Safi (Figs. 13-15), with the development of
942 RSBs above autochthonous salt attests the impact of pre-salt rift topography on salt
943 tectonics offshore Morocco. Movement over pre-salt relief generated earlier salt
944 structures that acted as weakness zones for later events (i.e. differential loading and
945 regional contraction), favouring the development of large volumes of allochthonous salt
946 sheets. This occurred to a greater extent in Essaouira, where salt thickness and
947 translation were greater (Figs. 7-8); demonstrating a positive relationship between
948 translation, salt thickness and supply for allochthonous salt.

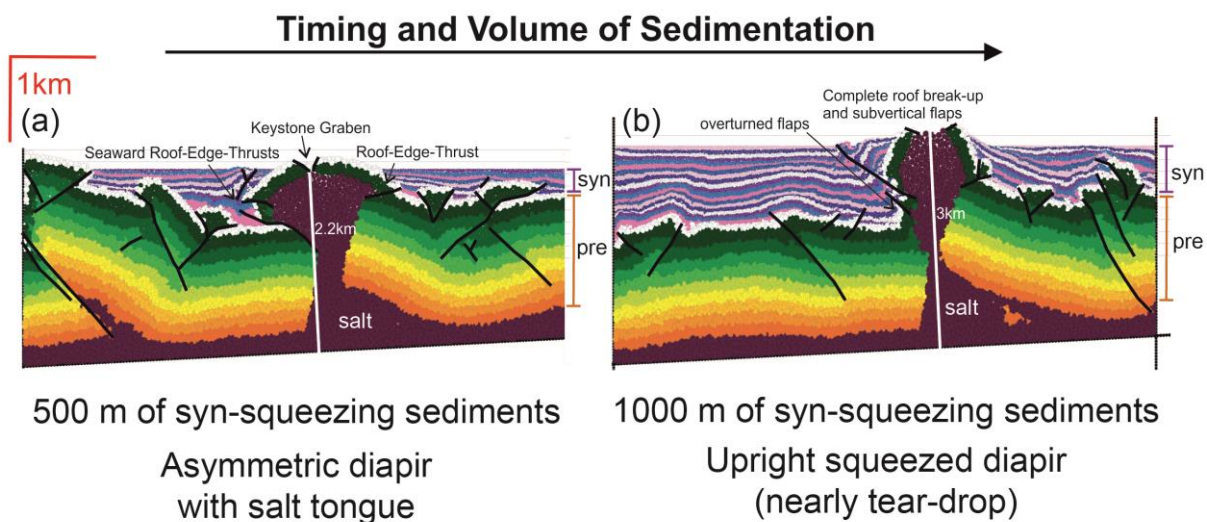
949 **7.3. Relationship between sediment input and structural style variations**

950 In addition to the initial salt thickness variation, differences in sediment input have also
951 been suggested to have a significant influence on along-strike structural style contrasts
952 (Tari et al., 2003; 2012; Tari and Jabour, 2013). Expanding on these pioneer studies, we
953 integrate seismic data with recently published numerical forward models to test the
954 effect of sedimentation on the growth of active diapirs (Fig. 22) (Pichel et al., 2017).

955 The largest contrast in thickness and sedimentation volume occurs within the Cenozoic
956 succession, which is thicker (c. 2-2.2 km) in Agadir and becomes thinner to the south,
957 being c. 1.6-1.7 km and 1-1.1 km thick on average in Essaouira and Safi, respectively
958 (compare figs. 5, 7 and 13-15). During this period, the main mechanism controlling salt
959 deformation was regional contraction as seen by the widespread occurrence of
960 squeezed diapirs along the entire margin (Figs. 5-8 and 16). Numerical models show the
961 relationship between sediment input and growth style of squeezed diapirs (Fig. 22),

962 producing similar geometries to those observed on the seismic data, especially when
 963 comparing them to the end-members scenarios of the thickest and thinnest syn-
 964 shortening interval of Agadir (Fig. 5) and Safi (Fig. 15). In these areas, the structural
 965 evolution is simpler and the volume of allochthonous salt smaller, allowing more
 966 confident analysis of the impact of sedimentation on growth of diapirs and,
 967 consequently, direct comparison with the models.

968 Where sediment input was higher, deformation was dominated by vertical movement;
 969 resulting in up-right squeezed diapirs c. 3-5 km tall (Figs. 5 and 22b). Where sediment
 970 input was half as thick, salt structures are shorter (c. 2-3.5 km), more asymmetric and
 971 characterized by seaward-leaning salt tongues (Figs. 13-15 and 22a). Thus, models
 972 support the earlier hypothesis that late variations in sediment input also acted as a
 973 significant control on along-strike variation of structural style along the margin (Tari et
 974 al., 2012; Tari and Jabour, 2013)



975

976 *Figure 22: Discrete-element models simulating rejuvenation of diapirs and syn-kinematic*
 977 *sedimentation testing the effects sediment input on the style of diapir growth (adapted from*
 978 *Pichel et al., 2017). These models are used to explain regional along-strike variation on style of late*
 979 *diapirism associated with shortening in the margin. (a) Low sediment input (500 m) results in*
 980 *lateral salt advance and development of allochthonous salt sheets such as in Safi where Late*
 981 *Cretaceous-Cenozoic sedimentation was the lowest. (b) High sediment input (1000 m) results in*

982 *generation of upright squeezed diapirs such as the ones in Agadir where Late Cretaceous-Cenozoic*
983 *sedimentation was approximately double that in Safi. Pre- and syn-kinematics sediments are*
984 *indicated in the model by hot and cold colours and lines at their right-hand side.*

985 **6.8. Conclusions**

986 The Moroccan Atlantic margin contains notoriously complex salt tectonics due to
987 significant variations in basin morphology, the syn-rift nature of the salt, the imprint of
988 oblique thick-skinned tectonics and contrasts in late sedimentation patterns. This work
989 shows that in the central and widest portion of the margin, the larger volume of salt
990 structures, greater translation and more complex kinematics reflect an originally
991 thicker salt and greater connectivity across multiple syn-rift structures. Further south,
992 in Agadir, less translation is observed and salt deformation is dominated by vertical
993 diapirism triggered by early downbuilding, followed by burial and late rejuvenation
994 driven by contraction and aided by the largest sediment input along the margin. The
995 northern segment, Safi, is narrower and has a smaller volume of salt structures,
996 suggesting salt was initially thinner. Translation, nevertheless, still occurred due to the
997 pronounced tilt (up to 10°) at base-salt level, but over a smaller area and number of pre-
998 salt structures resulting in simpler kinematically-linked gravity-driven system.

999 Allochthonous salt sheets developed at different times along the margin during four
1000 main phases from the Albian in Safi to Late Cretaceous, Paleocene to Oligo-Miocene in
1001 Essaouira. They become younger south- and basinward due to the combined influence
1002 of margin configuration, basement-involved contraction and volume of available salt.
1003 Albian sheets formed in Safi mainly by contraction at the downdip end of the salt basin
1004 against large pre-salt buffers; whereas Late Cretaceous-Paleocene sheets developed by
1005 two main mechanisms: differential loading and contraction. Distribution of these
1006 patterns varies along-dip and strike, with contraction-driven allochthons occurring

1007 occasionally updip of expulsion-driven ones, indicating an important control of pre-salt
1008 rift topography on salt deformation.

1009 We combined new 3D seismic data and numerical models to demonstrate that the
1010 alternation of structural domains and multiphase growth of diapirs and minibasins is
1011 caused by pre-salt rift topography and associated variable thickness of syn-rift salt. In
1012 Essaouira, where gliding was greater, the variations of supra-salt structural styles and
1013 influence of pre-salt rift topography were also greater than elsewhere. Base-salt relief
1014 also influenced flow at the allochthonous level, generating pairs of extensional-
1015 contractional zones with intermediate ramp-syncline basins. Despite the often limited
1016 resolution of the pre-salt syn-rift intervals, these complex supra-salt geometries can be
1017 used to estimate the location of base-salt and rift structures. This is useful for future
1018 seismic acquisition, processing and recognition of sub-salt structures, which represent
1019 prolific hydrocarbon plays worldwide.

1020 **Acknowledgments**

1021 The authors would like to thank Chris Jackson, Rob Gawthorpe, Neil Mitchell, Giovanni
1022 Bertotti and Andrew Newton for sharing their insights and criticism. We thank ONHYM
1023 and Kosmos for allowing us to use their seismic and well data offshore Morocco and
1024 especially for access to the 3D seismic data during a two-weeks visit to their
1025 headquarters. We also thank William Leslie from Kosmos for reviewing the final version
1026 of this manuscript and authorizing its publication. The main author would also like to
1027 thank the Science without Borders program and CNPQ, Brazil for sponsoring his PhD
1028 research. All authors would also like to thank the NARG sponsors: BP, Repsol, Equinor,
1029 Cairn, Woodside, Eni and Total for sponsoring part of this research. Schlumberger is
1030 also acknowledged for provision of Petrel software to the University of Manchester.

1031 **References**

1032 Adam, J., Krézsek, C., 2012. Basin-scale salt tectonic processes of the Laurentian Basin,
1033 Eastern Canada: insights from integrated regional 2D seismic interpretation and 4D
1034 physical experiments. Geological Society, London, Special Publications, 363(1), 331-360.

1035 Albertz, M., Beaumont, C., Shimeld, J. W., Ings, S. J., Gradmann, S., 2010. An investigation
1036 of salt tectonic structural styles in the Scotian Basin, offshore Atlantic Canada: 1.
1037 Comparison of observations with geometrically simple numerical models. Tectonics,
1038 29(4).

1039 Brown, A. R., 2011. Interpretation of three-dimensional seismic data. Society of
1040 Exploration Geophysicists and American Association of Petroleum Geologists.

1041 Brun, J. P., Fort, X., 2011. Salt tectonics at passive margins: Geology versus models.
1042 Marine and Petroleum Geology, 28(6), 1123-1145.

1043 Davison, I., 2005. Central Atlantic margin basins of North West Africa: geology and
1044 hydrocarbon potential (Morocco to Guinea). Journal of African Earth Sciences, 43(1-3),
1045 254-274.

1046 Davison, I., Anderson, L., Nuttall, P., 2012. Salt deposition, loading and gravity drainage
1047 in the Campos and Santos salt basins. Geological Society of London Special Publications,
1048 363(1), 159-174.

1049 Deptuck, M. E., Kendell, K. L., 2017. A review of Mesozoic-Cenozoic Salt Tectonics Along
1050 the Scotian Margin, Eastern Canada. In: Soto, J. I., Flinch, J., & Tari, G. (Eds.). (2017).
1051 Permo-Triassic Salt Provinces of Europe, North Africa and the Atlantic Margins:
1052 Tectonics and Hydrocarbon Potential. Elsevier, 287-312.

1053 Dooley, T. P., Hudec, M. R., & Jackson, M. P., 2012. The structure and evolution of sutures
1054 in allochthonous saltSalt Sutures. *AAPG bulletin*, 96(6), 1045-1070.

1055 Dooley, T. P., Jackson, M. P. A., & Hudec, M. R., 2015f. Breakout of squeezed stocks:
1056 Dispersal of roof fragments, source of extrusive salt and interaction with regional thrust
1057 faults. *Basin Research*, 27(1), 3-25.

1058 Dooley, T. P., Hudec, M. R., Carruthers, D., Jackson, M. P., Luo, G., 2016. The effects of
1059 base-salt relief on salt flow and suprasalt deformation patterns—Part 1: Flow across
1060 simple steps in the base of salt. *Interpretation*, 5(1), SD1-SD23.

1061 Dooley, T. P., Hudec, M. R., 2016. The effects of base-salt relief on salt flow and suprasalt
1062 deformation patterns—Part 2: Application to the eastern Gulf of Mexico. *Interpretation*,
1063 5(1), SD25-SD38.

1064 Dooley, T. P., Hudec, M. R., Pichel, L. M., Jackson, M. P., 2018. The impact of base-salt
1065 relief on salt flow and suprasalt deformation patterns at the autochthonous,
1066 paraautochthonous and allochthonous level: insights from physical models. *Geological*
1067 *Society, London, Special Publications*, 476, SP476-13.

1068 Dunlap, D. B., Wood, L. J., Weisenberger, C., Jabour, H., 2010. Seismic geomorphology of
1069 offshore Morocco's east margin, Safi Haute Mer area. *AAPG bulletin*, 94(5), 615-642.

1070 Ferrer, O., Jackson, M. P. A., Roca, E., Rubinat, M., 2012. Evolution of salt structures
1071 during extension and inversion of the Offshore Parentis Basin (Eastern Bay of Biscay).
1072 *Geological Society, London, Special Publications*, 363(1), 361-380.

1073 Ferrer, O., Gratacós, O., Roca, E., Muñoz, J. A., 2017. Modeling the interaction between
1074 presalt seamounts and gravitational failure in salt-bearing passive margins: The

1075 Messinian case in the northwestern Mediterranean Basin. *Interpretation*, 5(1), SD99-
1076 SD117.

1077 Frizon de Lamotte, D., Leturmy, P., Missenard, Y., Khomsi, S., Ruiz, G., Saddiqi, O.,
1078 Guillocheau, F., Michard, A., 2009. Mesozoic and Cenozoic vertical movements in the
1079 Atlas system (Algeria, Morocco, Tunisia): an overview. *Tectonophysics*, 475(1), 9-28.

1080 Ge, H., Jackson, M. P., Vendeville, B. C., 1997. Kinematics and dynamics of salt tectonics
1081 driven by progradation. *AAPG bulletin*, 81(3), 398-423.

1082 Hafid, M., Salem, A. A., Bally, A. W., 2000. The western termination of the Jebilet–High
1083 Atlas system (Offshore Essaouira Basin, Morocco). *Marine and Petroleum Geology*,
1084 17(3), 431-443.

1085 Hafid, M., Zizi, M., Bally, A. W., Salem, A. A., 2006. Structural styles of the western
1086 onshore and offshore termination of the High Atlas, Morocco. *Comptes Rendus*
1087 *Geoscience*, 338(1-2), 50-64.

1088 Hudec, M. R., Jackson, M. P., 2004. Regional restoration across the Kwanza Basin, Angola:
1089 Salt tectonics triggered by repeated uplift of a metastable passive margin. *AAPG*
1090 *bulletin*, 88(7), 971-990.

1091 Hudec, M. R., Jackson, M. P., 2006. Advance of allochthonous salt sheets in passive
1092 margins and orogens. *AAPG bulletin*, 90(10), 1535-1564.

1093 Hudec, M. R., Jackson, M. P., 2007. Terra infirma: Understanding salt tectonics. *Earth-*
1094 *Science Reviews*, 82(1-2), 1-28.

1095 Hudec, M. R., Jackson, M. P., Schultz-Ela, D. D., 2009. The paradox of minibasin
1096 subsidence into salt: Clues to the evolution of crustal basins. Geological Society of
1097 America Bulletin, 121(1-2), 201-221.

1098 Hudec, M. R., Norton, I. O., Jackson, M. P., Peel, F. J., 2013. Jurassic evolution of the Gulf of
1099 Mexico salt basin. AAPG bulletin, 97(10), 1683-1710.

1100 Ings, S. J., Shimeld, J. W., 2006. A new conceptual model for the structural evolution of a
1101 regional salt detachment on the northeast Scotian margin, offshore eastern Canada.
1102 AAPG bulletin, 90(9), 1407-1423.

1103 Jabour, H., Dakki, M., Nahim, M., Charrat, F., El Alji, M., Hssain, M., Oumalch., El Abibi, R.,
1104 2004. The Jurassic depositional system of Morocco, geology and play concepts. MAPG
1105 Mem, 1, 5-39.

1106 Jackson, M. P., Hudec, M. R., 2005. Stratigraphic record of translation down ramps in a
1107 passive-margin salt detachment. Journal of Structural Geology, 27(5), 889-911.

1108 Jackson, M.P., Hudec, M.R., 2017. Salt Tectonics: Principles and Practice. Cambridge
1109 University Press.

1110 Jackson, C. A. L., Jackson, M. P., Hudec, M. R., 2015a. Understanding the kinematics of
1111 salt-bearing passive margins: A critical test of competing hypotheses for the origin of
1112 the Albian Gap, Santos Basin, offshore Brazil. Geological Society of America Bulletin,
1113 127(11-12), 1730-1751.

1114 Jackson, C. A. L., Jackson, M. P., Hudec, M. R., Rodriguez, C. R., 2015b. Enigmatic
1115 structures within salt walls of the Santos Basin—Part 1: Geometry and kinematics from
1116 3D seismic reflection and well data. Journal of Structural Geology, 75, 135-162.

- 1117 Jansa, L. F., Wiedmann, J., 1982. Mesozoic-Cenozoic development of the Eastern North
1118 American and Northwest African continental margins: a comparison. In *Geology of the*
1119 *northwest African continental margin* (pp. 215-269). Springer, Berlin, Heidelberg.
- 1120 Jones, I. F., Davison, I., 2014. Seismic imaging in and around salt bodies. *Interpretation*,
1121 2(4), SL1-SL20.
- 1122 Krézsek, C., Adam, J., Grujic, D., 2007. Mechanics of fault and expulsion rollover systems
1123 developed on passive margins detached on salt: insights from analogue modelling and
1124 optical strain monitoring. *Geological Society, London, Special Publications*, 292(1), 103-
1125 121.
- 1126 Lancelot, Y., Winterer, E. L., 1980. Evolution of the Moroccan oceanic basin and adjacent
1127 continental margin—a synthesis. *Initial Reports of the Deep Sea drilling project*, 50,
1128 801-821.
- 1129 Luber, T., 2017 *Integrated Analysis of Lower Cretaceous Stratigraphy And Depositional*
1130 *Systems: The Essaouira-Agadir Basin Of Morocco* (Unpublished doctoral dissertation).
1131 University of Manchester, Manchester, United Kingdom.
- 1132 Luber, T. L., Bulot, L. G., Redfern, J., Nahim, M., Jeremiah, J., Simmons, M. Bodin, S., Frau,
1133 C., Bidgood, M., Masrour, M. 2019. A revised chronostratigraphic framework for the
1134 Aptian of the Essaouira-Agadir Basin, a candidate type section for the NW African
1135 Atlantic Margin. *Cretaceous Research*, 93, 292-317.
- 1136 Le Roy, P., Piqué, A., 2001. Triassic–Liassic Western Moroccan synrift basins in relation
1137 to the Central Atlantic opening. *Marine Geology*, 172(3-4), 359-381.

1138 McClay, K. R., 1990. Extensional fault systems in sedimentary basins: a review of
1139 analogue model studies. *Marine and petroleum Geology*, 7(3), 206-233.

1140 McClay, K. R., 1996. Recent advances in analogue modelling: uses in section
1141 interpretation and validation. Geological Society, London, Special Publications, 99(1),
1142 201-225.

1143 McClay, K., Shaw, J. H., & Suppe, J., 2011. Thrust Fault-Related Folding: AAPG Memoir 94
1144 (Vol. 94). AAPG.

1145 Neumaier, M., Back, S., Littke, R., Kukla, P. A., Schnabel, M., Reichert, C., 2016. Late
1146 Cretaceous to Cenozoic geodynamic evolution of the Atlantic margin offshore Essaouira
1147 (Morocco). *Basin Research*, 28(5), 712-730.

1148 Peel, F. J., 2014a. How do salt withdrawal minibasins form? Insights from forward
1149 modelling, and implications for hydrocarbon migration. *Tectonophysics*, 630, 222-235.

1150 Peel, F. J., 2014b. The engines of gravity-driven movement on passive margins:
1151 Quantifying the relative contribution of spreading vs. gravity sliding mechanisms.
1152 *Tectonophysics*, 633, 126-142.

1153 Pichel, L. M., Finch, E., Huuse, M., Redfern, J., 2017. The influence of shortening and
1154 sedimentation on rejuvenation of salt diapirs: A new Discrete-Element Modelling
1155 approach. *Journal of Structural Geology*, 104, 61-79.

1156 Pichel, L.M., Peel, F., Jackson, C.A.-L., Huuse, M., 2018, Geometry and kinematics of salt-
1157 detached ramp syncline basins, *Journal of Structural Geology*, 115, 208-230. , doi:
1158 10.1016/j.jsg.2018.07.016.

1159 Pichel, L. M., Finch, E., Gawthorpe, R., 2018. The Impact of Pre-salt Rift Topography on
1160 Salt Tectonics: a Discrete-Element Modelling Approach.

1161 Quirk, D. G., Schødt, N., Lassen, B., Ings, S. J., Hsu, D., Hirsch, K. K., Von Nicolai, C. (2012).
1162 Salt tectonics on passive margins: examples from Santos, Campos and Kwanza basins.
1163 Geological Society, London, Special Publications, 363(1), 207-244.

1164 Roma, M., Ferrer, O., Roca, E., Pla, O., Escosa, F. O., Butillé, M., 2018. Formation and
1165 inversion of salt-detached ramp-syncline basins. Results from analog modeling and
1166 application to the Columbrets Basin (Western Mediterranean). *Tectonophysics*, 745,
1167 214-228.

1168 Rowan, M. G., & Weimer, P., 1998. Salt-sediment interaction, northern Green Canyon and
1169 Ewing bank (offshore Louisiana), northern Gulf of Mexico. *AAPG bulletin*, 82(5), 1055-
1170 1082.

1171 Rowan, M. G., Jackson, M. P., Trudgill, B. D., 1999. Salt-related fault families and fault
1172 welds in the northern Gulf of Mexico. *AAPG bulletin*, 83(9), 1454-1484.

1173 Rowan, M. G., Peel, F. J., Vendeville, B. C., 2004. Gravity-driven fold belts on passive
1174 margins. In: McClay, K.R. (Ed.), *Thrust Tectonics and Hydrocarbon Systems*. AAPG
1175 Memoir, vol. 82, pp. 157-182.

1176 Rowan, M.G., 2014. Passive-margin salt basins: hyperextension, evaporite deposition,
1177 and salt tectonics. *Basin Research*, 26(1), 154-182.

1178 Rowan, M. G., 2018. The South Atlantic and Gulf of Mexico salt basins: crustal thinning,
1179 subsidence and accommodation for salt and presalt strata. Geological Society, London,
1180 Special Publications, 476, SP476-6.

1181 Saura, E., Vergés, J., Martín-Martín, J. D., Messenger, G., Moragas, M., Razin, P., rélaud, C.,
1182 Joussiaume, R., Malaval, M., Homke, S., Hunt, D. W., 2014. Syn-to post-rift diapirism and
1183 minibasins of the Central High Atlas (Morocco): the changing face of a mountain belt.
1184 *Journal of the Geological Society*, 171(1), 97-105.

1185 Schuster, D. C., 1995. Deformation of allochthonous salt and evolution of related salt-
1186 structural systems, eastern Louisiana Gulf Coast, in: Jackson, M. P. A., Roberts, D.G.,
1187 Snelson, S. (Eds.), *Salt Tectonics: a Global Perspective*. AAPG Memoir, vol. 65, pp. 177-
1188 198.

1189 Shaw, J. H., Connors, C. D., & Suppe, J., 2005. Seismic interpretation of contractional
1190 fault-related folds: An AAPG seismic atlas (Vol. 53). American Association of Petroleum
1191 Geologists.

1192 Steiner, C., Hobson, A., Favre, P., Stampfli, G. M., Hernandez, J., 1998. Mesozoic sequence
1193 of Fuerteventura (Canary Islands): Witness of Early Jurassic sea-floor spreading in the
1194 central Atlantic. *Geological Society of America Bulletin*, 110(10), 1304-1317.

1195 Tari, G., Molnar, J., Ashton, P., Hedley, R., 2000. Salt tectonics in the Atlantic margin of
1196 Morocco. *The Leading Edge*, 19(10), 1074-1078.

1197 Tari, G., Molnar, J., Ashton, P., 2003. Examples of salt tectonics from West Africa: a
1198 comparative approach. *Geological Society, London, Special Publications*, 207(1), 85-104.

1199 Tari, G., Molnar, J., 2005. Correlation of syn-rift structures between Morocco and Nova
1200 Scotia, Canada. In *Transactions GCSSEPM Foundation, 25th Ann. Res. Conf* (pp. 132-
1201 150).

1202 Tari, G., Jabour, H., Molnar, J., Valasek, D., Zizi, M., 2012a. Deep-water Exploration in
1203 Atlantic Morocco: Where Are the Reservoirs? *in* D. Gao, ed., *Tectonics and*
1204 *sedimentation: Implications for petroleum systems: AAPG Memoir 100*, p. 337–355.

1205 Tari, G., Brown, D., Jabour, H., Hafid, M., Louden, K., Zizi, M., 2012b. The conjugate
1206 margins of Morocco and Nova Scotia. In *Regional geology and tectonics: Phanerozoic*
1207 *passive margins, cratonic basins and global tectonic maps* (pp. 284-323).

1208 Tari, G., Jabour, H., 2013. Salt tectonics along the Atlantic margin of Morocco. *Geological*
1209 *Society, London, Special Publications*, 369(1), 337-353.

1210 Tari, G., Novotny, B., Jabour, H., Hafid, M., 2017. Salt tectonics along the Atlantic Margin
1211 of NW Africa (Morocco and Mauritania). In: Soto, J. I., Flinch, J., & Tari, G. (Eds.). (2017).
1212 *Permo-Triassic Salt Provinces of Europe, North Africa and the Atlantic Margins:*
1213 *Tectonics and Hydrocarbon Potential*. Elsevier, 331-351

1214 Vendeville, B. C., Jackson, M. P. A., 1992b. The fall of diapirs during thin-skinned
1215 extension. *Marine and Petroleum Geology*, 9(4), 354-371.

1216 Vergés, J., Moragas, M., Martín-Martín, J. D., Saura, E., Casciello, E., Razin, P., Grélaud, C.,
1217 Malaval, M., Jousiame, R., Messenger, G., Sharp, I. 2017. Salt tectonics in the Atlas
1218 mountains of Morocco. In *Permo-Triassic Salt Provinces of Europe, North Africa and the*
1219 *Atlantic Margins* (pp. 563-579).

1220 Weatherall, P., Marks, K. M., Jakobsson, M., Schmitt, T., Tani, S., Arndt, J. E., et al. (2015).
1221 A new digital bathymetric model of the world's oceans. *Earth and Space Science*, 2(8),
1222 331–345